PURDUE RESEARCH FOUNDATION
Project Nos. 5250 and 5567

TECHNICAL REPORT FMTR-70-2
December 1970

SHOCK INDUCED BOUNDARY LAYER OVER A SEMI-INFINITE FLAT PLATE

Part II

Complete Problem

by

Douglas E. Abbott and Michael I. O. Ero

SCHOOL OF MECHANICAL ENGINEERING
FLUID MECHANICS GROUP
PURDUE UNIVERSITY

Technical Report FMTR 70-2

December 1970

NATIONAL AERONAUTICS AND SPACE ADMINISTRATION
Grant No. NGR 15-005-077

SHOCK INDUCED BOUNDARY LAYER OVER A SEMI-INFINITE FLAT PLATE

Part II

Complete Problem

by

Douglas E. Abbott and Michael I. O. Ero

PURDUE RESEARCH FOUNDATION

Project No. 5250 and 5567

NATIONAL AERONAUTICS AND SPACE ADMINISTRATION

Grant No. NGR 15-005-077

School of Mechanical Engineering
Fluid Mechanics Group
Purdue University

Technical Report FMTR-70-2

December 1970

ABSTRACT

The complete problem of shock induced boundary-layer flow on a semi-infinite flat plate is analyzed. A previous analysis which considered the flow only in the immediate vicinity of the shock wave was extended to include leading edge effects and served as the basis of the present study. Calculations are shown for this truly unsteady problem for both a perfect gas and a real gas in thermodynamic equilibrium. Results are presented for the boundary-layer growth as a function of time for various shock wave intensities. It is shown that the predicted asymptotic approach of the leading-edge flow to steady state values (as the shock wave moves farther and farther along the plate) agrees very well with experimental results based on wall heat transfer measurements made by Felderman and Davies and Bernstein. Results are also shown for the skin-friction coefficient and the Nusselt number for a range of shock intensities and shock wave locations.

ACKNOWLEDGMENTS

The authors wish to acknowledge Purdue University for providing computer funds during the early phases of this work and NASA-Ames Research Center for their support under Grant 15-005-077. In particular, thanks are given to Mr. M. W. Rubesin and Mr. L. L. Presley of NASA-Ames for their help and constructive criticism at various stages of the work, and to Professors F. P. Incropera and F. J. Marshall and Doctors Koob and Deiwert for their valuable discussions. The work on which this report is based has been updated from the Ph.D. Thesis of Dr. M. I. O. Ero, completed in March, 1968.

TABLE OF CONTENTS

LIST OF SYMBOLS

C_f - Skin friction coefficient, $\left(\mu \frac{\partial u}{\partial y}\right)_{y=0} \Big/ \rho_e U_e^2$

g_c - Gravitational constant, 32.174 ft/sec^2

h - Dimensional static enthalpy, Btu/lbm

J - Joule mechanical equivalent of heat, 778.16 ft-lbf/Btu

L - Characteristic length, feet

P - Static pressure outside boundary layer

Pr - Prandtl number $\mu C_p/K$

Re_L - Reynolds number defined by $\rho_e U_e L/\mu_e$

t - Time, seconds

u - Velocity parallel to flat plate

v - Transverse velocity

w - The ratio of velocities across a stationary normal shock

y - Transverse independent variable

Greek Letters

δ - Boundary-layer thickness, equation (4.1c)

δ^* - Displacement thickness, equation (4.1d)

δ^{**} - Momentum thickness, equation (4.1e)

δ^{***} - Energy dissipation thickness, equation (4.1f)

η - Nondimensional transverse coordinate, $\sqrt{U_e/\nu_e L}\ y$

μ - Dynamic viscosity

ν - Kinematic viscosity

ϕ - Nondimensional transport variable, $\rho\mu/\rho_e\mu_e$

ρ - Density

ξ - Nondimensional longitudinal variable, x/L

τ - Nondimensional time variable, $U_e t/L$

θ - Inverse of the gradient of the nondimensional velocity given by $(\partial u^*/\partial \eta)^{-1}$

Subscripts and Superscripts

e - Variable evaluated outside the boundary layer

i - Indexing subscript as in h_o, h_1, etc.

L - Characteristic length of flat plate

n - Nodal index

w - Value of a variable evaluated at the wall

* - Denotes variable nondimensionalized with respect to its value at the outer edge of the boundary layer in plate fixed coordinates

1. INTRODUCTION

The complete problem of shock induced boundary-layer flow on a semi-infinite flat plate will be considered in this report. In a companion report [1], the flow was analyzed in the immediate vicinity of a plane shock wave moving over a flat plate into a gas initially at rest. This previous analysis will now be extended to include the leading edge effect on the flow and a solution will be sought which joins the leading edge problem to the shock-vicinity problem into a complete and continuous unsteady boundary-layer analysis. As in the earlier work [1], the semi-infinite flat plate will be assumed to model a shock-tube splitter plate and the laminar boundary-layer equations with zero pressure gradient will be considered to adequately represent the flow (a discussion of solutions of the Navier-Stokes equations at the leading edge for incompressible flow may be found in [2]).

The flow under consideration is shown for three locations of the shock wave in Figure 1. As shown in the figure, time is measured relative to the shock passing the leading edge of the plate. In keeping with reference [1], it is assumed that there is no attenuation of the shock wave and the gas will be assumed either to be perfect or a real gas in thermodynamic equilibrium. Also, in accordance with the earlier work, the variation of thermodynamic variables such as density and

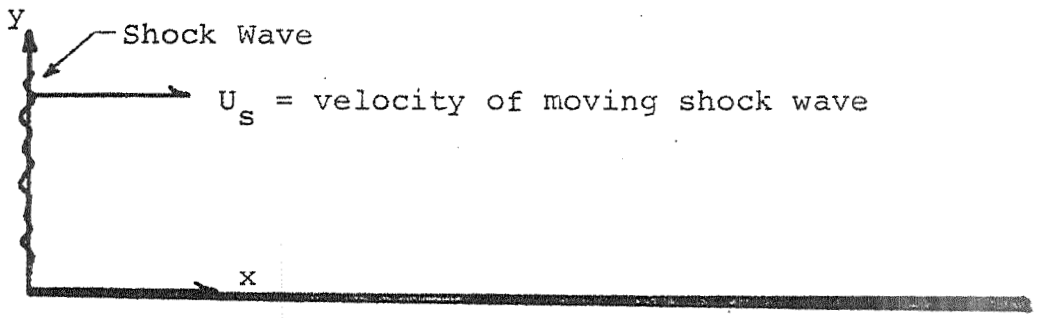

a. Shock arrives at the flat plate leading edge, t = 0.

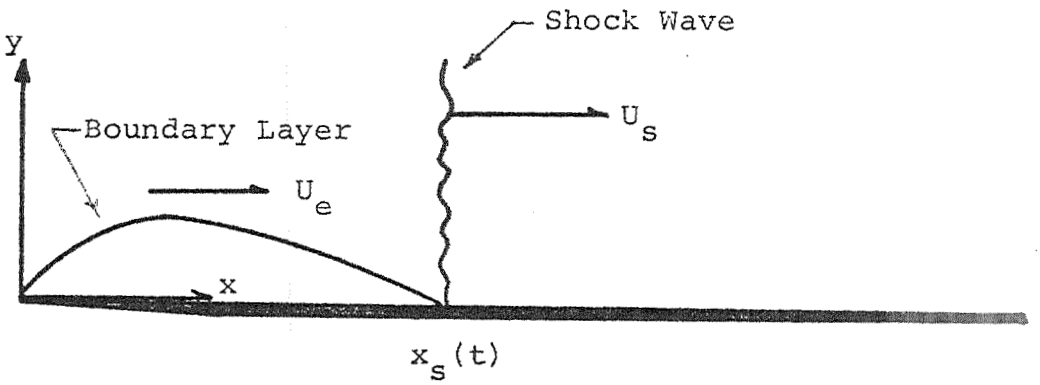

b. Location of the shock for t > 0.

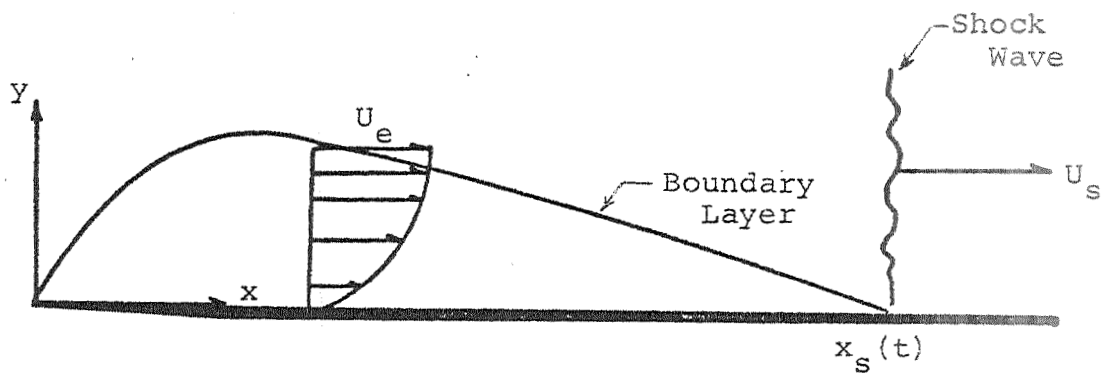

c. Location of the shock at a later time.

Figure 1. Shock Induced Flow On a Semi-Infinite Flat Plate.

enthalpy are assumed to be monotonic across the boundary layer.

In reference [1], the method of weighted residuals or MWR was employed as an analytical method for solving the appropriate equations. It was found, for example, that an MWR first approximation was accurate to within about 6 percent of the solution for wall shear stress given by Lam and Crocco [3], while a second approximation agreed to better than one percent. It is on this basis that the more complicated problem to be treated here (i.e., including the leading edge effects) will incorporate the MWR technique in a second approximation together with a finite difference method for analyzing the complete unsteady flow.

2. MATHEMATICAL FORMULATION

The flow under consideration is a laminar two-dimensional boundary layer generated by a plane shock wave moving over a semi-infinite flat plate, see Figure 1. Relative to the plate, the shock wave is located a distance $x_s(t)$ from the leading edge, where $x_s(t) = U_s t$ and U_s is the velocity of the shock relative to the plate. In keeping with reference [1], the following assumptions are made:

(i) The shock wave is plane, attached to the plate, and does not attenuate with time.

(ii) The conditions outside the boundary layer behind the moving shock wave are adequately related to the conditions ahead of the shock by the Rankine-Hugoniot relation for a normal shock.

(iii) The boundary layer is laminar, at constant pressure, and is adequately described by the classical two-dimensional unsteady boundary-layer equations for a compressible flow.

(iv) The fluid is considered to be either a perfect gas with constant Prandtl number, or a real gas in thermodynamic equilibrium.

In addition to these four assumptions, conditions at the leading edge must be specified. An extensive survey of the leading edge problem for incompressible flow is given in

reference [2]; this review shows that as long as low density slip flow effects are not encountered, and as long as the unit Reynolds number is greater than about 10 per foot, the leading edge of the plate is felt upstream a distance of the order of $3\sqrt{\nu t}$. Thus, for typical pressures and temperatures normally occurring in shock tube applications, it is adequate for engineering purposes to apply the classical boundary-layer assumptions to the leading edge without alteration. Thus, a final assumption becomes:

(v) The boundary-layer equations adequately describe the flow in the vicinity of the plate leading edge, the leading edge itself being a mathematical singular point in the classical fashion.

Under the above assumptions, the following governing equations are obtained for flow relative to the plate:

Continuity

$$\frac{\partial \rho}{\partial t} + \frac{\partial \rho u}{\partial x} + \frac{\partial \rho v}{\partial y} = 0 \tag{2.1}$$

Momentum

$$\rho \frac{\partial u}{\partial t} + \rho u \frac{\partial u}{\partial x} + \rho v \frac{\partial u}{\partial y} = \frac{\partial}{\partial y}\left(\mu \frac{\partial u}{\partial y} \right) \tag{2.2}$$

$$\frac{\partial P}{\partial y} = 0 \tag{2.3a}$$

$$\frac{\partial P}{\partial x} = 0 \text{ (flat plate case)} \tag{2.3b}$$

Energy

$$\rho \frac{\partial h}{\partial t} + \rho u \frac{\partial h}{\partial x} + \rho v \frac{\partial h}{\partial y} = \frac{\partial}{\partial y}\left(\frac{\mu}{Pr} \frac{\partial h}{\partial y} \right) + \frac{\mu}{g_c J}\left(\frac{\partial u}{\partial y} \right)^2 \tag{2.4}$$

The thermodynamic and transport property relations are assumed in the form:

$$\rho = \rho(h)$$
$$\mu = \mu(h) \qquad (2.5)$$
$$Pr = Pr(h)$$

The boundary conditions for velocity and static enthalpy are:

$$u(x > x_s, y, t) = 0 \qquad (2.6a)$$
$$v(x > x_s, y, t) = 0 \qquad (2.6b)$$
$$u(x, 0, t) = 0 \qquad (2.6c)$$
$$v(x, 0, t) = 0 \qquad (2.6d)$$
$$u(x, y \to \infty, t) \to U_e \qquad (2.6e)$$
$$u(x_s, y > 0, t) = U_e \qquad (2.6f)$$
$$h(x > x_s, y, t) = h_w \qquad (2.6g)$$
$$h(x, 0, t) = h_w \qquad (2.6h)$$
$$h(x, y \to \infty, t) \to h_e \qquad (2.6i)$$
$$h(x_s, y > 0, t) = h_e \qquad (2.6j)$$

where u is the longitudinal velocity parallel to, and v is the transverse velocity perpendicular to, the plate, respectively. It will also be assumed that the wall temperature remains constant during the flow. Thus

$$h_w = \text{constant} \qquad (2.6k)$$

This last assumption can be justified by the large thermal capacity of the splitter plate and the short duration of shock tube flows. The initial and leading-edge conditions are:

$$u(x,y,0) = 0 \tag{2.6ℓ}$$

$$v(x,y,0) = 0 \tag{2.6m}$$

$$h(x,y,0) = h_w \tag{2.6n}$$

$$u(0,y>0,t) = U_e \tag{2.6o}$$

$$v(0,y>0,t) = 0 \tag{2.6p}$$

$$h(0,y>0,t) = h_e \tag{2.6q}$$

It is convenient to normalize the dependent variables in equations (2.1) to (2.6) with respect to their values in the freestream, and to define nondimensional independent variables as follows:

$$u^* = \frac{u}{U_e} \tag{2.7a}$$

$$v^* = v\sqrt{\frac{L}{\nu_e U_e}} \tag{2.7b}$$

$$h^* = \frac{h}{h_e} \tag{2.7c}$$

$$\rho^* = \frac{\rho}{\rho_e} \tag{2.7d}$$

$$\mu^* = \frac{\mu}{\mu_e} \tag{2.7e}$$

$$\phi = \rho^*\mu^* \tag{2.7f}$$

$$\xi = \frac{x}{L} \tag{2.7g}$$

$$\eta = \sqrt{\frac{U_e}{\nu_e L}}\, y \tag{2.7h}$$

$$\tau = \frac{U_e t}{L} \tag{2.7i}$$

where L is an arbitrary reference length. Under the above transformation, the governing equations become:

Continuity

$$\frac{\partial \rho^*}{\partial \tau} + \frac{\partial \rho^* u^*}{\partial \xi} + \frac{\partial \rho^* v^*}{\partial \eta} = 0 \tag{2.8}$$

Momentum

$$\rho^* \frac{\partial u^*}{\partial \tau} + \rho^* u^* \frac{\partial u^*}{\partial \xi} + \rho^* v^* \frac{\partial u^*}{\partial \eta} = \frac{\partial}{\partial \eta}\left(\mu^* \frac{\partial u^*}{\partial \eta}\right) \tag{2.9}$$

Energy

$$\rho^* \frac{\partial h^*}{\partial \tau} + \rho^* u^* \frac{\partial h^*}{\partial \xi} + \rho^* v^* \frac{\partial h^*}{\partial \eta} = \frac{\partial}{\partial \eta}\left(\frac{\mu^*}{Pr} \frac{\partial h^*}{\partial \eta}\right) + \frac{U_e^2}{g_c J h_e} \mu^* \left(\frac{\partial u^*}{\partial \eta}\right)^2 \tag{2.10}$$

Property equations

$$\rho^* = \rho^*(h^*) \tag{2.11a}$$

$$\mu^* = \mu^*(h^*) \tag{2.11b}$$

$$Pr = Pr(h^*) \tag{2.11c}$$

Boundary conditions:

$$u^*(\xi > \xi_s, \eta, \tau) = 0 \tag{2.12a}$$

$$v^*(\xi > \xi_s, \eta, \tau) = 0 \tag{2.12b}$$

$$u^*(\xi, 0, \tau) = 0 \tag{2.12c}$$

$$v^*(\xi, 0, \tau) = 0 \tag{2.12d}$$

$$u^*(\xi, \eta \to \infty, \tau) \to 1 \tag{2.12e}$$

$$u^*(\xi_s, \eta > 0, \tau) = 1 \tag{2.12f}$$

$$h^*(\xi > \xi_s, \eta, \tau) = h_w/h_e \tag{2.12g}$$

$$h^*(\xi, 0, \tau) = h_w/h_e \tag{2.12h}$$

$$h^*(\xi, \eta \to \infty, \tau) \to 1 \tag{2.12i}$$

$$h^*(\xi_s, \eta > 0, \tau) = 1 \tag{2.12j}$$

Initial and leading-edge conditions:

$$u^*(\xi,\eta,0) = 0 \tag{2.12k}$$

$$v^*(\xi,\eta,0) = 0 \tag{2.12ℓ}$$

$$h^*(\xi,\eta,0) = h_w/h_e \tag{2.12m}$$

$$u^*(0,\eta>0,\tau) = 1 \tag{2.12n}$$

$$v^*(0,\eta>0,\tau) = 0 \tag{2.12o}$$

$$h^*(0,\eta>0,\tau) = 1 \tag{2.12p}$$

Equations (2.8), (2.9), and (2.10) are partial differential equations in the three independent variables, ξ, η, and τ. Solutions were obtained to these equations in reference [1] for the immediate vicinity of the shock wave, that is, subject to boundary conditions (2.12a) through (2.12j). However, when the leading edge is taken into account, the initial and leading-edge conditions, equations (2.12k) through (2.12p), must be applied and the solution becomes much more complex. The complete solution to be considered in this report, that is, including the leading-edge effects, will build upon the previous results of reference [1]. The next section will briefly review the analysis and results of the shock-vicinity analysis, and then will describe how these previous results are incorporated into the complete analysis.

3. ANALYSIS

In reference [1], the governing equations and boundary conditions (2.8) to (2.10) and (2.12a) to (2.12j) were solved in the vicinity of the shock wave by employing the method of weighted residuals or MWR to reduce the number of independent variables from three to two. The resulting calculations for an MWR second approximation were compared with Mirels' solutions [4] for a perfect gas and showed agreement within one percent for the skin-friction coefficient. On the basis of this close agreement, the MWR second approximation of reference [1] will be employed to extend the analysis to the leading-edge problem.

The full details of the MWR analysis are given in reference [1] and will not be repeated here. Briefly, however, the following steps are taken: Equations (2.8) and (2.9) are combined by suitably employing a weighting function and the resulting equation is integrated across the boundary layer. The independent variable η is changed to u by introducing the function

$$\theta = \left(\frac{\partial u^*}{\partial \eta}\right)^{-1}$$

Similar steps are taken with the energy equation, (2.10). The dependent variables which appear in the resulting equations are then represented by an N-th order approximation.

For a second approximation, N=2, the expressions become

$$\rho^*\theta \simeq \frac{1}{1-u^*}\left[(1-2u^*)\ \rho_o\theta_o + u^*\rho_1\theta_1\right] \tag{3.1a}$$

$$h^* \simeq a_o + a_1 u^* + a_2 u^{*2} \tag{3.1b}$$

where

$$a_o = h_o = h_w/h_e \tag{3.2a}$$

$$a_1 = -3h_o + 4h_1 - 1 \tag{3.2b}$$

$$a_2 = 2h_o - 4h_1 + 2 \tag{3.2c}$$

The parameters $\rho_i\theta_i$ and h_i for $i = 0,1$ are unknown functions of τ and ξ and are determined by solving the following two equations for $\rho_o\theta_o$ and $\rho_1\theta_1$ (in matrix form)

$$\begin{bmatrix} (\rho_o\theta_o)^{\cdot} \\ (\rho_1\theta_1)^{\cdot} \end{bmatrix} = \begin{bmatrix} -\frac{1}{3} & \frac{1}{6} \\ \frac{1}{3} & -\frac{2}{3} \end{bmatrix} \begin{bmatrix} (\rho_o\theta_o)' \\ (\rho_1\theta_1)' \end{bmatrix} + \begin{bmatrix} 8 & -8 \\ 2 & 0 \end{bmatrix} \begin{bmatrix} \frac{\phi_o}{\rho_o\theta_o} \\ \frac{\phi_1}{\rho_1\theta_1} \end{bmatrix} \tag{3.3}$$

and h_1 is determined from the equation (note that h_o is specified solely from the boundary conditions which determine h_w and h_e).

$$\frac{\partial h_1}{\partial \tau} = \Bigg\{ -a_0 \frac{(\rho_0\theta_0)^{\cdot}}{2} - a_1\left[-\frac{1}{6}(\rho_0\theta_0)^{\cdot} + \frac{1}{3}(\rho_1\theta_1)^{\cdot}\right] - a_2\left[-\frac{1}{6}(\rho_0\theta_0)^{\cdot} + \frac{1}{4}(\rho_1\theta_1)^{\cdot}\right] - \left(-\frac{1}{15}\rho_0\theta_0 + \frac{1}{5}\rho_1\theta_1\right)\frac{\partial h_1}{\partial \xi} - a_0\left[-\frac{1}{6}(\rho_0\theta_0)' + \frac{1}{3}(\rho_1\theta_1)'\right] - a_1\left[-\frac{1}{6}(\rho_0\theta_0)' + \frac{1}{4}(\rho_1\theta_1)'\right] - a_2\left[-\frac{3}{20}(\rho_0\theta_0)' + \frac{1}{5}(\rho_1\theta_1)'\right] - a_1\left(\frac{\phi}{Pr}\right)_0 \frac{1}{\rho_0\theta_0} + a_0\left(\frac{\phi_0}{\rho_0\theta_0}\right) + a_1\left[\frac{1}{6}\frac{\phi_0 + \left(\frac{\phi}{Pr}\right)_0}{\rho_0\theta_0} + \frac{2}{3}\frac{\phi_1 + \left(\frac{\phi}{Pr}\right)_1}{\rho_1\theta_1}\right] + \frac{2}{3}a_2\left(\frac{\phi_1 + \left(\frac{\phi}{Pr}\right)_1}{\rho_1\theta_1}\right) + \frac{U_e^2}{g_c J h_e}\left(\frac{1}{6}\frac{\phi_0}{\rho_0\theta_0} + \frac{1}{3}\frac{\phi_1}{\rho_1\theta_1}\right)\Bigg\} \Bigg/ \left(\frac{3}{\rho_1\theta_1}\right) \qquad (3.4)$$

In these two equations, the dots represent differentiation with respect to τ and the primes differentiation with respect to ξ. The thermodynamic property variables appearing in equations (3.3) and (3.4), ϕ_i and $(\phi/Pr)_i$, are functions of the enthalpy field within the boundary layer: specifically they are determined by a collocation procedure given in reference [1]. The boundary and initial conditions (2.12) become:

$$\rho_i\theta_i(\xi=0,\tau\geq 0) = 0 \qquad (3.5a)$$

$$\rho_i\theta_i(\xi=\xi_s(\tau),\tau\geq 0) = 0 \qquad (3.5b)$$

for i = 0,1 and

$$h_1(\xi=0,\tau\geq 0) = 1 \qquad (3.5c)$$

$$h_1(\xi=\xi_s(\tau),\tau\geq 0) = 1 \qquad (3.5d)$$

Equations (3.3) and (3.4) are nonlinear partial differential equations in the two independent variables τ and ξ. It was shown in reference [1] that for a perfect gas with ϕ_o and ϕ_1 constant, it is possible to obtain an analytic solution to equation (3.3) in the vicinity of the shock wave; this solution is given by

$$\rho_i \theta_i = A_i \sqrt{\frac{4\phi_i}{2\frac{U_s}{U_e} - 1}\left(\frac{U_s}{U_e}\tau - \xi\right)} \qquad (3.6)$$

where the constant coefficients A_i are found by iteration of equation (3.3). However, it is not possible to obtain such a solution for either a perfect or real gas when the leading edge condition (3.5a) is employed. Thus, a numerical approach will be taken and solutions will be sought by considering an appropriate finite difference technique.

3.1 Finite Difference Formulation

The range of the independent variable ξ may be taken to be $0 \leq \xi \leq 1$ since the reference length L is completely arbitrary. However, the nondimensionalized time variable takes values from zero when the shock wave arrives at the leading edge of the flat plate to a value which in general is determined by the arrival of the contact surface. From a purely computational standpoint, however, τ may be assumed to vary from zero to infinity. For this reason, it is convenient to reformulate the governing equations by finite differencing the independent variable which has a finite absolute range, and

to treat the resulting difference equations as a system of simultaneous ordinary differential equations for which a solution may be found by solving for the dependent variables at all the nodal points.

Let the nodal point located at the n-th position have a coordinate (ξ_n,τ) given by

$$\xi_n = \xi_{n-1} + \Delta\xi_{n-1}$$

Then the nodal points given by

$$\xi_{n-1} = \xi_{n-2} + \Delta\xi_{n-2} \tag{3.7a}$$

and

$$\xi_{n+1} = \xi_n + \Delta\xi_n \tag{3.7b}$$

(for n=1,2,3,...) will be designated the neighboring nodes of the point at ξ_n. In equations (3.7), the distance between the n-th and the (n+1)-th nodes is equal to the local step size $\Delta\xi_n$. In general, the internodal distance need not be constant, but in this study a constant step size will be assumed. Thus the maximum number of nodes spanning the length L of the flat plate is given by

$$N_{max} = 1/\Delta\xi + 1 \tag{3.8}$$

in which the first node is located at the leading edge. It will be recalled that at $\tau=0$, the shock wave just arrives at the leading edge, n=1, and as the flow progresses (i.e., at any time greater than zero) the shock location determines the point $\xi=\xi_s(\tau)$ with nodal number n_s beyond which no flow exists.

Thus at those nodal points downstream of n_s the gas is "unaware" of the flow; therefore, the nodes for which finite-difference equations need to be written are given by

$$1 < n < \frac{\xi_s}{\Delta\xi} + 1 \tag{3.9}$$

It is evident from equation (3.9) that the first node, $\xi_{n=1}$, has only right-hand neighbors, and any node n_s at the foot of the moving shock wave has only left-hand neighbors. The values of $\rho_i\theta_i$ and h_i at the node n will be denoted by $\rho_i\theta_i\ (\tau,n)$ and $h_i\ (\tau,n)$ respectively.

The following equations are the finite difference system which approximates equations (3.3) and (3.4). The derivatives of the dependent variables with respect to ξ will be approximated by a central difference

$$\frac{\partial}{\partial\xi}[\rho_i\theta_i(\tau,\xi_n)] \approx \frac{\rho_i\theta_i(\tau,\xi_{n+1}) - \rho_i\theta_i(\tau,\xi_{n-1})}{2\Delta\xi} + O(\Delta\xi^2) \tag{3.10a}$$

for $i = 0, 1$

and

$$\frac{\partial}{\partial\xi}[h_1(\tau_n\xi_n)] \approx \frac{h_1(\tau,\xi_{n+1}) - h_2(\tau,\xi_{n-1})}{2\Delta\xi} + O(\Delta\xi^2) \tag{3.10b}$$

In the case of the end nodes (those having neighbors only on one side), the derivatives may be approximated by a forward difference:

$$\frac{\partial}{\partial\xi}[\rho_i\theta_i(\tau,\xi_{n_s})] \approx \frac{\rho_i\theta_i(\tau,\xi_{n_s}) - \rho_i\theta_i(\tau,\xi_{n_s-1})}{\Delta\xi} \tag{3.11}$$

Introducing equations (3.10) into equations (3.3) and (3.4) yields the following equations:

$$\begin{bmatrix} (\rho_0\theta_0) \\ (\rho_1\theta_1)^{\cdot} \end{bmatrix} = \frac{1}{2\Delta\xi} \begin{bmatrix} -\frac{1}{3} & \frac{1}{6} \\ \frac{1}{3} & -\frac{2}{3} \end{bmatrix} \begin{bmatrix} \rho_0\theta_0(\tau,\xi_{n+1}) - \rho_0\theta_0(\tau,\xi_{n-1}) \\ \rho_1\theta_1(\tau,\xi_{n+1}) - \rho_1\theta_1(\tau,\xi_{n-1}) \end{bmatrix}$$

$$+ \begin{bmatrix} 8 & -8 \\ 2 & 0 \end{bmatrix} \begin{bmatrix} \frac{\phi_0(\tau,\xi_n)}{\rho_0\theta_0(\tau,\xi_n)} \\ \frac{\phi_1(\tau,\xi_n)}{\rho_1\theta_1(\tau,\xi_n)} \end{bmatrix} + O(\Delta\xi^2) \qquad (3.12)$$

and

$$h_1(\tau,\xi_n)^{\cdot} = \left[-\frac{a_0}{2}\rho_0\theta_0(\tau,\xi_n)^{\cdot} - a_1\left[-\frac{1}{6}\rho_0\theta_0(\tau,\xi_n)^{\cdot} + \frac{1}{3}\rho_1\theta_1(\tau,\xi_n)^{\cdot}\right] - a_2\left[-\frac{1}{6}\rho_0\theta_0(\tau,\xi_n)^{\cdot} + \frac{1}{4}\rho_1\theta_1(\tau,\xi_n)^{\cdot}\right]\right.$$

$$- \frac{1}{2\Delta\xi}\left[-\frac{1}{15}\rho_0\theta_0(\tau,\xi_n) + \frac{1}{5}\rho_1\theta_1(\tau,\xi_n)\right]\left[h_1(\tau,\xi_{n+1}) - h_1(\tau,\xi_{n-1})\right] - \frac{a_0}{2\Delta\xi}\left\{-\frac{1}{6}\left[\rho_0\theta_0(\tau,\xi_{n+1}) - \rho_0\theta_0(\tau,\xi_{n-1})\right]\right.$$

$$\left. + \frac{1}{3}\left[\rho_1\theta_1(\tau,\xi_{n+1}) - \rho_1\theta_1(\tau,\xi_{n-1})\right]\right\} - \frac{a_1}{2\Delta\xi}\left\{-\frac{1}{6}\left[\rho_0\theta_0(\tau,\xi_{n+1}) - \rho_0\theta_0(\tau,\xi_{n-1})\right] + \frac{1}{4}\left[\rho_1\theta_1(\tau,\xi_{n+1}) - \rho_1\theta_1(\tau,\xi_{n-1})\right]\right\}$$

$$- \frac{a_2}{2\Delta\xi}\left\{-\frac{3}{20}\left[\rho_0\theta_0(\tau,\xi_{n+1}) - \rho_0\theta_0(\tau,\xi_{n-1})\right] + \frac{1}{4}\rho_1\theta_1(\tau,\xi_{n+1})\right.$$

$$-\rho_1\theta_1(\tau,\xi_{n-1})\Big]\Big\} - a_1\left(\frac{\phi(\tau,\xi_n)}{Pr}\right)\frac{1}{\rho_0\theta_0(\tau,\xi_n)} + a_0\frac{\phi_0(\tau,\xi_n)}{\rho_0\theta_0(\tau,\xi_n)}$$

$$+a_1\left[\frac{1}{6}\,\frac{\phi_0(\tau,\xi_n)+\left(\frac{\phi}{Pr}(\tau,\xi_n)\right)_1}{\rho_0\theta_0(\tau,\xi_n)} + \frac{2}{3}\,\frac{\phi_1(\tau,\xi_n)+\left(\frac{\phi}{Pr}(\tau,\xi_n)\right)_1}{\rho_1\theta_1(\tau,\xi_n)}\right]$$

$$+\frac{2}{3}a_2\frac{\phi_1(\tau,\xi_n)+\left(\frac{\phi}{Pr}(\tau,\xi_n)\right)_1}{\rho_1\theta_1(\tau,\xi_n)} + \frac{U_e^2}{g_c J h_e}\left(\frac{1}{6}\,\frac{\phi_0(\tau,\xi_n)}{\rho_0\theta_0(\tau,\xi_n)}\right.$$

$$\left.+\frac{1}{3}\,\frac{\phi_1(\tau,\xi_n)}{\rho_0\theta_0(\tau,\xi_n)}\right)\Bigg]\Bigg/\left(\frac{3}{\rho_1\theta_1(\tau,\xi_n)}\right) \qquad (3.13)$$

The variables a_0, a_1, a_2 are defined for each nodal point as follows:

$$a_o = h_o \qquad (3.14a)$$

$$a_1 = -3h_o + 4h_1(\tau,\xi_n) - 1 \qquad (3.14b)$$

$$a_2 = 2h_o - 4h_1(\tau,\xi_n) + 2 \qquad (3.14c)$$

The boundary and initial conditions become

$$\rho_i\theta_i(\tau\geq 0, n=1) = 0 \qquad (3.15a)$$

$$\rho_i\theta_i(\tau>0, n=n_s) = 0 \qquad (3.15b)$$

and

$$h_1(\tau\geq 0, n=1) = 1 \qquad (3.15c)$$

In equations (3.12) and (3.13), when $\xi_n = \xi_{n_s}$, the nodal index n_s specifies the current location of the moving shock wave. Because the flow does not exist at those nodal points for which the nodal index n is greater than n_s, the integration of equations (3.12) and (3.13) with respect to τ is performed for n_s-2 nodes. It is clear from (3.9) and (3.15) that no integration needs be performed for the nodes at n=1 and

$n=n_s$. It may be noted that the magnitude of the nodal index $n=n_s$ increases as the shock advances from its initial position at the leading edge, n=1, to its maximum value given by N_{max} in equation (3.8) when the shock wave arrives at the point x = L. It follows therefore that at the end of an integration interval, the number by which n_s is increased is proportional to the nondimensional time step-size and the velocity of propagation of the wavefront; that is, for any given $\Delta\tau$ step size, the increment in the range of the flat plate affected by the flow is proportional to the shock wave velocity.

3.2 Starting the Solution

A difficulty which needs to be resolved in starting the solution of the unsteady problem in the entire region affected by the flow is that of providing a realistic estimate of values of the dependent variables for small times. Since the dependent variables $\rho_i\theta_i$, i=0,1 occur as reciprocals in the reduced momentum and energy equations, the initial conditions given in equation (3.15a) with $\rho_i\theta_i(\xi,0)=0$ are unsatisfactory for starting numerical integration. Thus several features of this flow need to be considered in order to obtain a physically meaningful starting formulation. In addition to the continuous axial expansion of the boundary-layer flow on the plate, it may be noted that for small times the distance between the leading edge and the foot of the shock wave is in general small and its magnitude is determined by the velocity of the moving shock wave. This is an important feature of this flow which

distinguishes it from the similar problem of a flat plate suddenly accelerated or impulsively moved in a surrounding fluid initially at rest. In fact, for the suddenly-accelerated plate case, all gradients of velocity and temperature are zero before the inception of the flow, but these gradients are finite for any small time greater than zero since the flow exists everywhere on the plate (the gradients can be estimated from the related shock-vicinity problem in coordinates fixed relative to the shock wave, the "Rayleigh" problem). In the present shock induced leading-edge problem, however, not only are the dependent variables to be estimated for small times, it is clear that the estimate must be made in a short axial region bounded by the leading edge and the foot of the shock wave.

In reference [1], it was shown that a sufficiently accurate evaluation of the dependent variables $\rho_i \theta_i$ and h_1 can be obtained in the shock-vicinity or "Rayleigh" region of the flow. In the present leading-edge problem, it is possible to identify a "Rayleigh" region which at any time ends at the foot of the moving shock wave and extends upstream at least to a point where $\xi=\tau$ (further upstream of this point, the flow will "feel" the leading edge). It is also reasonable to propose that, after the shock wave moves past the leading edge, the flow characteristics of the boundary layer at the leading edge and stations downstream of it will develop continuously with time. At some intermediate point, the region of the flow controlled by the leading edge should uniformly

blend into the region of the flow influenced by the location of the moving shock. For computational reasons, it is necessary to enforce a transition condition on the dependent variables such that at the match point, the dependent variables and their gradients must approach the same value from both upstream and downstream. Thus the point $\xi=\tau$ is not a singularity in the normal sense of the term; it represents a point across which the governing equations cannot be applied in their original form without imposing an auxillary smoothing condition. This is a direct result, of course, of the boundary-layer equations being parabolic rather than elliptic partial differential equations.

In this study, the values of $\rho_i\theta_i$ were estimated in the "Rayleigh" region by means of the analytic perfect gas solution derived in reference [1], that is equation (3.6), together with equation (3.1a) and the solution given by Mirels [4], as modified by Lam and Crocco [3], in the form:

$$\rho_o\theta_o = \sqrt{\frac{6\phi_o^2}{2.82\,\frac{U_s}{U_e} - 1}\left(\frac{U_s}{U_e}\,\tau - \xi\right)} \qquad (3.16)$$

Specifically, the constants A_o and A_1 of equation (3.6) were determined from equation (3.1a) evaluated at $u^*=0$ and $u^*=1/2$, respectively, with the left hand side of (3.1a) assumed to be given by the first approximation

$$\rho^*\theta \simeq \frac{\rho_o\theta_o}{1-u^*} \qquad (3.17)$$

evaluated using equation (3.16). The resulting estimates for A_i, substituted into (3.6), are assumed to provide the starting values for $\rho_o\theta_o$ and $\rho_1\theta_1$ in the "Rayleigh" region, $\tau \leq \xi \leq \xi_s$, for $\xi_s = 0.1$. The corresponding leading edge values, $0 \leq \xi \leq \tau$, were obtained by fitting a polynomial of the form

$$\rho_i\theta_i(\xi,\tau_o) = c_o + c_1\sqrt{\xi} + c_2\xi \tag{3.18}$$

such that

$$\lim_{\varepsilon\to 0} \rho_i\theta_i(\xi,\tau_o-\varepsilon) = \lim_{\varepsilon\to 0} \rho_i\theta_i(\xi,\tau_o+\varepsilon) \tag{3.19a}$$

$$\lim_{\varepsilon\to 0} \frac{\partial}{\partial\xi} \rho_i\theta_i(\xi,\tau_o-\varepsilon) = \lim_{\varepsilon\to 0} \frac{\partial}{\partial\xi} \rho_i\theta_i(\xi,\tau_o+\varepsilon) \tag{3.19b}$$

where

$$\tau_o = \xi_s \frac{(w-1)}{w}$$

and w is the velocity ratio across a normal stationary shock,

$$w = \frac{U_s}{U_s - U_e}$$

The conditions prescribed in equations (3.19) ensure a smooth transition between the leading-edge region and the "Rayleigh" region, and thus provide the simultaneous equations required for calculating the coefficients in equation (3.18).

The starting conditions given by the above procedure not only provide the nonzero values of $\rho_i\theta_i$ which are required for computational reasons, but properly describe the leading-edge and "Rayleigh" region variation for the initial position

of the shock wave. The selection of the starting location of the shock is arbitrary, but the final choice is such that the flow duration associated with the shock at $\xi_s = 0.1$ is less that ten percent of the total calculated flow time. In addition it is necessary to minimize the initial value of ξ_s in order to obtain a satisfactory polynomial fit for the leading edge region.

3.3 Continuing the Solution

The computation of the dependent variables $\rho_i\theta_i$ and h_1 for increasing time is obtained by numerical integration of equations (3.12) and (3.13) at each nodal point using a fourth order Runga-Kutta method. The choice of internodal step size and time step size was made not only to ensure that the behavior of $\rho_i\theta_i$ is consistent with the model,

$$\rho_i\theta_i(\xi,\tau\geq 0) \geq 0 \tag{3.20}$$

but also because the time and longitudinal space coordinates are constrained such that

$$t = x_s/U_s$$

or in nondimensional valiables

$$\tau = \xi_s(w-1)/w \tag{3.21}$$

The time increment is thus obtained as

$$\Delta\tau = \Delta\xi(w-1)/w \tag{3.22}$$

Hence, by choosing $\Delta\xi$, $\Delta\tau$ is determined from (3.22). The

choice for $\Delta\xi$ is made such that the inequality (3.20) is satisfied at each node point for all time. A value of $\Delta\xi = 0.01$ was found to be the most satisfactory.

In the physical domain, with $\Delta\xi = 0.01$, the corresponding time step size is equivalent to the time it takes the shock wavefront to traverse one percent of the total length L. While this constraint may be too severe in the case of weak shocks, it has distinct advantages for high intensity shocks; for increasing shock intensities, the time step size is decreasing, thus assuring a reasonable time resolution of the rate of growth of the dependent variables at each node. Perhaps the best criterion for stability of the solution is given by equation (3.20); in this study it was used as the basis for discarding those step-sizes which yielded inconsistent results.

The computation for the time dependence of the variables $\rho_o\theta_o$, $\rho_1\theta_1$ and h_1 at each node was obtained by integrating (3.12) and (3.13) repeatedly for all nodal points n in the range $2 \leq n \leq n_s - 1$. The node n_s corresponds to the current location of the shock wave, and at the end of each integration n_s is increased by one. The node $n_s - 1$ always lies in the "Rayleigh" region, therefore its starting values can be estimated as described above in Section 3.2. The resulting calculations, then, are a combined MWR second approximation and finite difference solution. Results were obtained for the appropriate boundary-layer parameters and are presented in the next section for both a perfect and a real gas.

4. CALCULATED RESULTS

The solutions for $\rho_o\theta_o$, $\rho_1\theta_1$, and h_1 obtained from the finite difference equations (3.12) and (3.13) by the method described in the last section are substituted into equations (3.1a) and (3.1b) to yield the approximate solution for $\rho^*\theta$ and h^* as a function of τ and ξ. In obtaining these calculations, the thermodynamic and transport variables ρ^*, ϕ, and ϕ/Pr are related to h^* by polynomial curve fitting with the coefficients evaluated by a collocation procedure: the details are given in reference [1]. The thermodynamic equilibrium real gas calculations reported here were made for nitrogen using the transport and thermodynamic properties of Ahtye and Peng [5] as curve fit by Marvin and Deiwert [6]; again the details including tabular values, are given in reference [1]. All of the results reported here were made assuming an initial pressure of 0.001 atm and an initial temperature of 530°R. For the perfect gas calculations, $\phi=1$ and $Pr = 0.72$ were assumed.

The standard boundary-layer parameters may be computed from the following definitions:

Skin-friction coefficient:

$$C_f\sqrt{Re_L} = \frac{\left(\mu \frac{\partial u}{\partial y}\right)_{y=0}}{\rho_e U_e^2}\sqrt{Re_L} = \frac{\phi_o}{\rho_o\theta_o} \qquad (4.1a)$$

Velocity profile:

$$\frac{Y}{L}\sqrt{Re_L} = \int_0^{u^*} \theta \, du^* \tag{4.1b}$$

Boundary-layer thickness:

$$\frac{\delta}{L}\sqrt{Re_L} = \int_0^{U_e^*} \theta \, du^* \tag{4.1c}$$

Displacement thickness:

$$\frac{\delta^*}{L}\sqrt{Re_L} = \int_0^{U_e^*} \theta(1-\rho^* u^*) \, du^* \tag{4.1d}$$

Momentum thickness:

$$\frac{\delta^{**}}{L}\sqrt{Re_L} = \int_0^{U_e^*} \rho^* \theta u^* (1-u^*) \, du^* \tag{4.1e}$$

Energy dissipation thickness:

$$\frac{\delta^{***}}{L}\sqrt{Re_L} = \int_0^{U_e^*} \rho^* \theta u^* (1-u^{*2}) \, du^* \tag{4.1f}$$

Nusselt number:

$$\frac{Nu(1-h_o)}{Re_L} = \frac{1}{\theta_o}\left(\frac{\partial h^*}{\partial u^*}\right)_{u^*=0} \tag{4.1g}$$

In these relations, $Re_L = U_e L/\nu_e$ and U_e^* is arbitrarily taken as $U_e^* = 0.995$.

The development of the boundary-layer thickness is shown in figure 2 for the perfect gas case, and in figure 3 for the

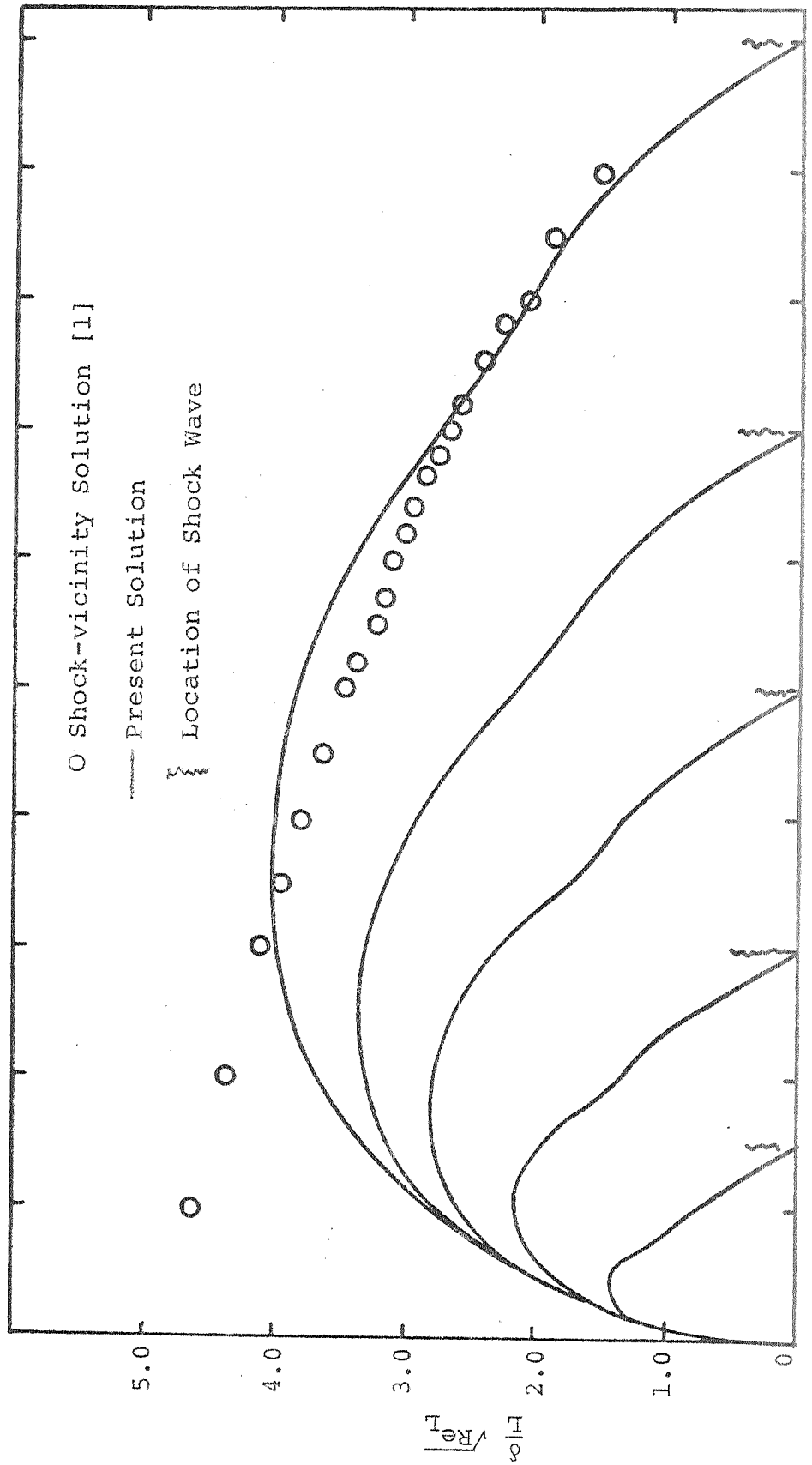

Figure 2. Boundary-Layer Thickness as a Function of Shock Wave Position; Perfect Gas, $M_s = 3.15$.

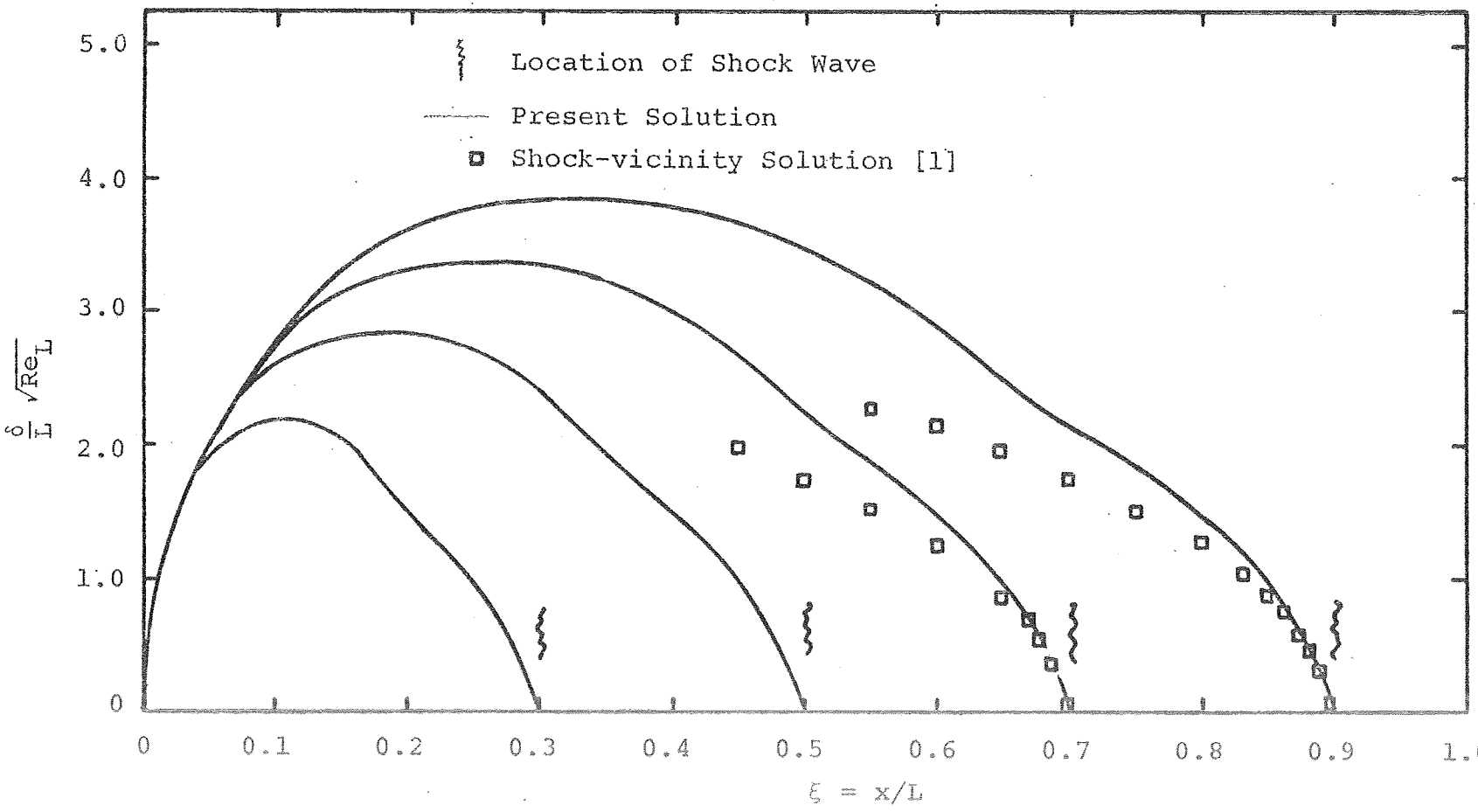

Figure 3. Boundary-Layer Thickness Parameter as a Function of Shock Wave Position; Real Gas, $M_s = 3.15$.

case in which the transport and thermodynamic properties are evaluated from the real gas properties tabulated for nitrogen. Figures 2 and 3 show the manner of propagation of the leading edge effect as the shock wave moves down the plate. The region affected by the leading edge asymptotically increases with the downstream movement of the shock wave. This observation applies to all intensities of the moving shock. The comparison shown in figures 2 and 3 shows agreement with the shock-vicinity analysis of reference [1] in the region close to the shock wave. The deviation between the two solutions increases with distance away from the shock. The reason for the unexpected waviness in the calculated curves downstream of the maximum value is not known at present, however it is probably a result of the numerical smoothing procedure at the $\tau=\xi$ point (this will be investigated in future studies).

Figure 4 shows the boundary-layer thickness parameter at that instant when the moving shock wave is located at 0.99 L for different values of the shock wave Mach number, M_s. Unfortunately, the boundary-layer thickness parameter given by equation (4.1c) tends to conceal the physical variation of the boundary-layer thickness δ with shock wave Mach number M_s because of the manner in which the Reynolds number $Re_L = U_e L/\nu_e$ enters the calculation. To illustrate this point, figure 4 is replotted in figure 5 by assuming L is one foot and calculating the Reynolds number for the appropriate real gas properties. Figure 5 shows that the boundary layer is in fact becoming thinner with increasing shock intensities.

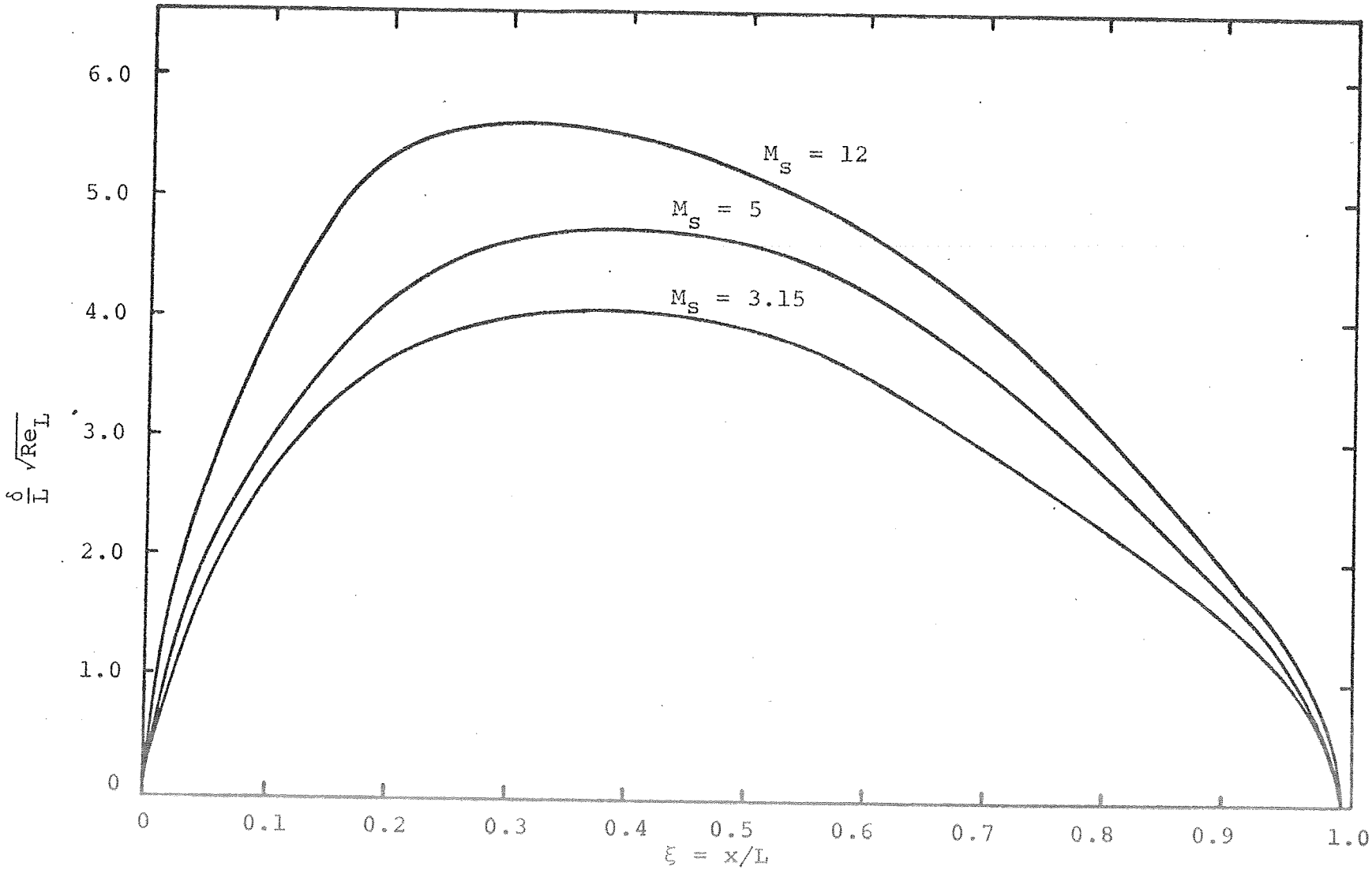

Figure 4. Boundary-Layer Thickness Parameter as a Function of Shock Wave Intensity; Real Gas.

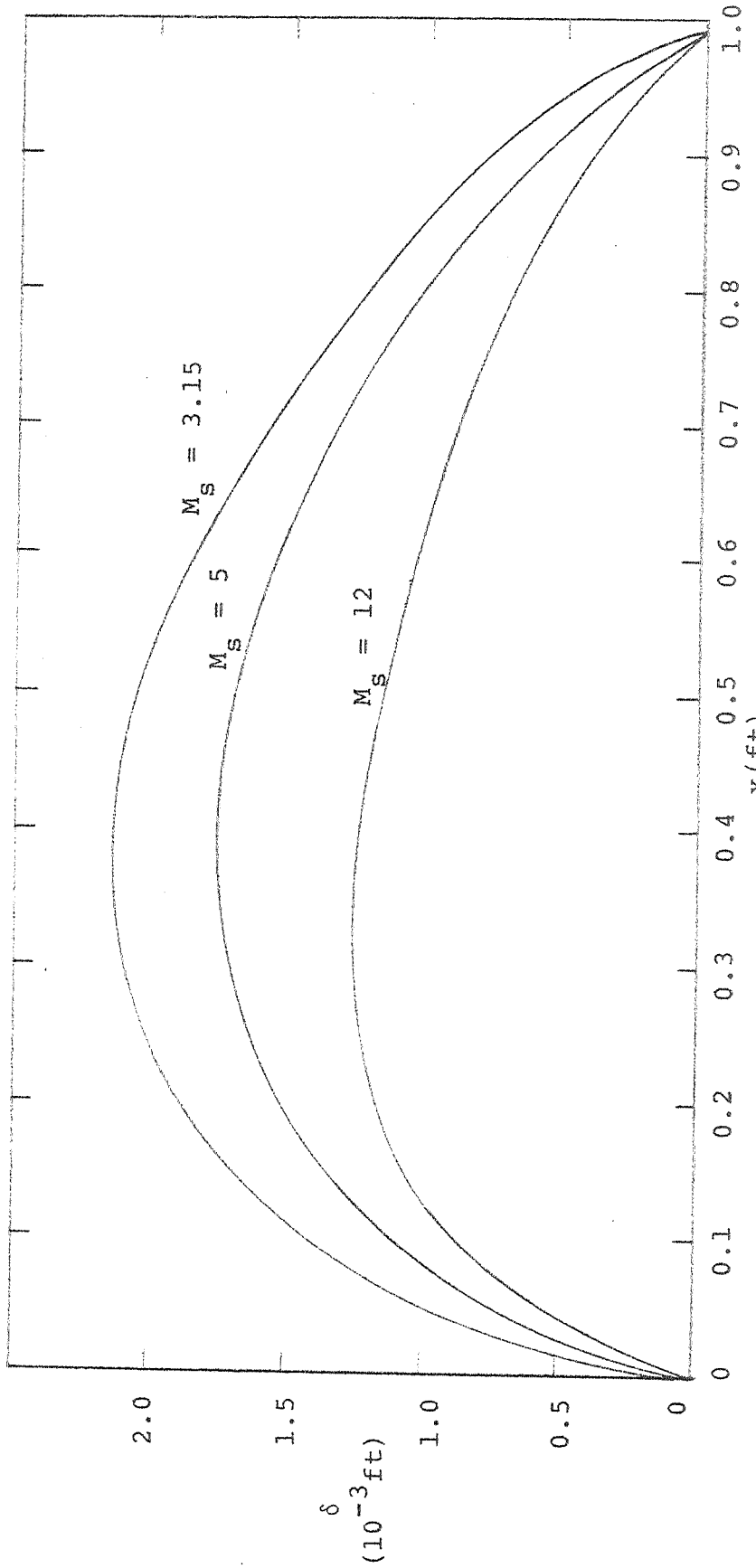

Figure 5. Boundary-Layer Thickness as a Function of Shock Wave Intensity (Assuming L = 1 ft.); Real Gas.

It may be noted from figures 2 and 3 that the present solution, accounting for the leading edge, is significantly different than the shock-vicinity solution of reference [1] except quite close to the shock wave. From a slightly different viewpoint, these figures show that the majority of the flow is truly unsteady, except for the steady flow asymptote resulting from the leading edge conditions (i.e., the Blasius flow asymptote, which is the "exact" long-time solution). The asymptotic approach of the leading-edge flow to a steady state condition is given in figure 6. These curves are defined as the locus of points in space and time at which the boundary-layer thickness has reached 95 percent of its steady state value. Similar results have been obtained experimentally by Felderman [7] and Davies and Bernstein [8] based on wall heat transfer measurements. The present results are compared with the experimental values in figure 7 where it is seen that the agreement is very satisfactory over most of the range of the present calculations.

Figure 8 shows a comparison of skin friction results obtained for the complete flow and the shock-vicinity analyses for $M_s = 1.6$. Again the agreement with the shock-vicinity model is good near the shock wave and a progressively increasing departure is observed as the leading edge is approached. It is also seen that, as expected, there is no essential difference between a perfect and a real gas calculation. Figure 9 shows the skin friction distribution for two positions of the moving shock wave for a perfect gas and $M_s = 2.2$. In figure

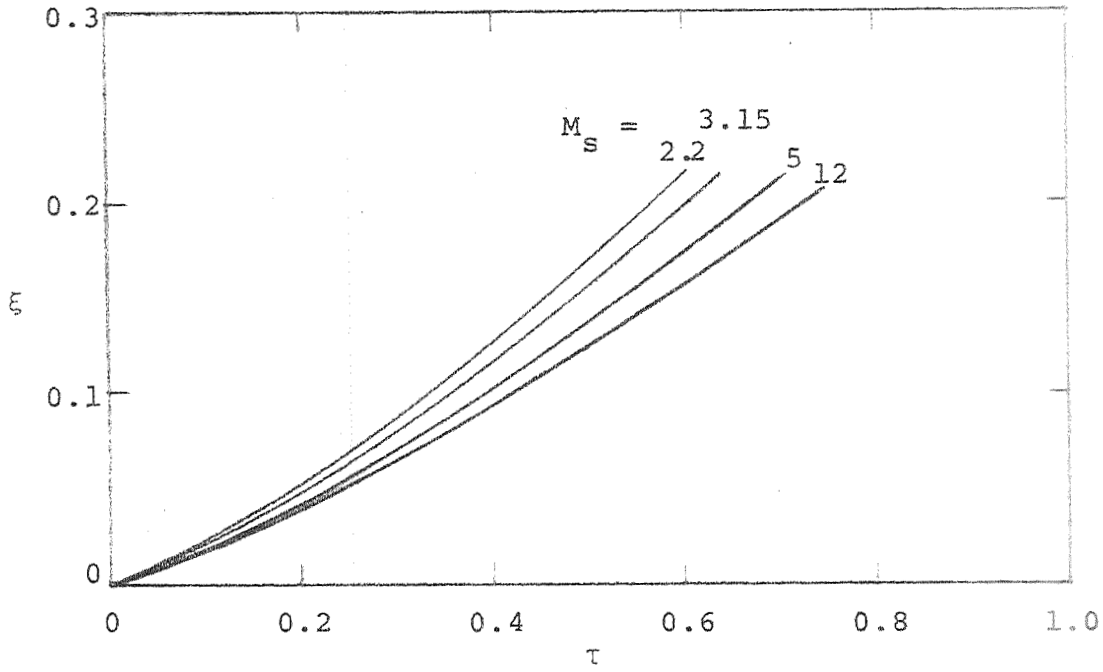

Figure 6. Locus of Points in Time and Space at Which the Boundary-Layer Thickness Reaches 95 Percent of its Steady State Value; Real Gas.

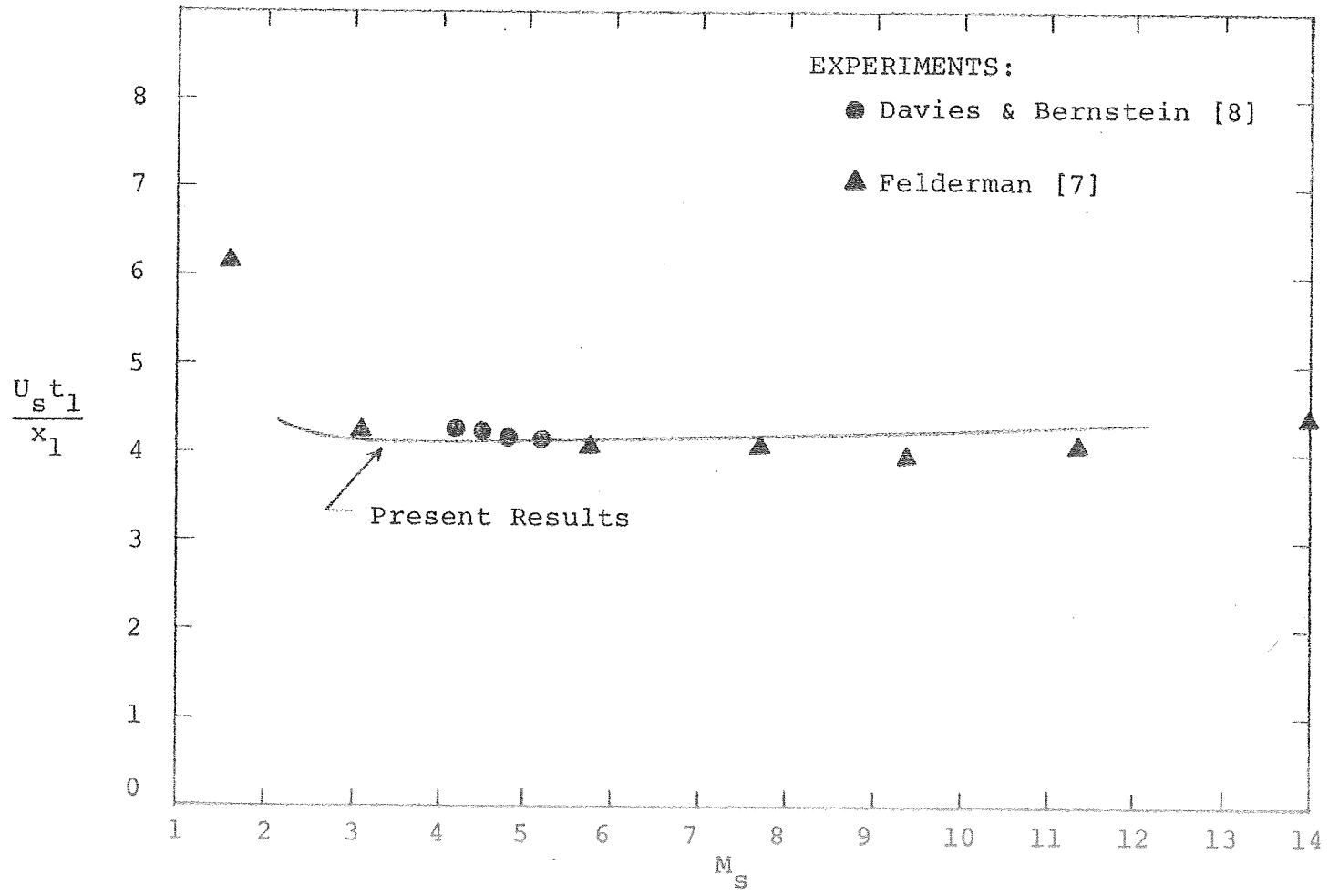

Figure 7. Elapsed Time t_1 for a Boundary Layer to Reach Steady-State, Versus Shock Mach Number (x_1 = Point of Measurement on the Plate) Real Gas.

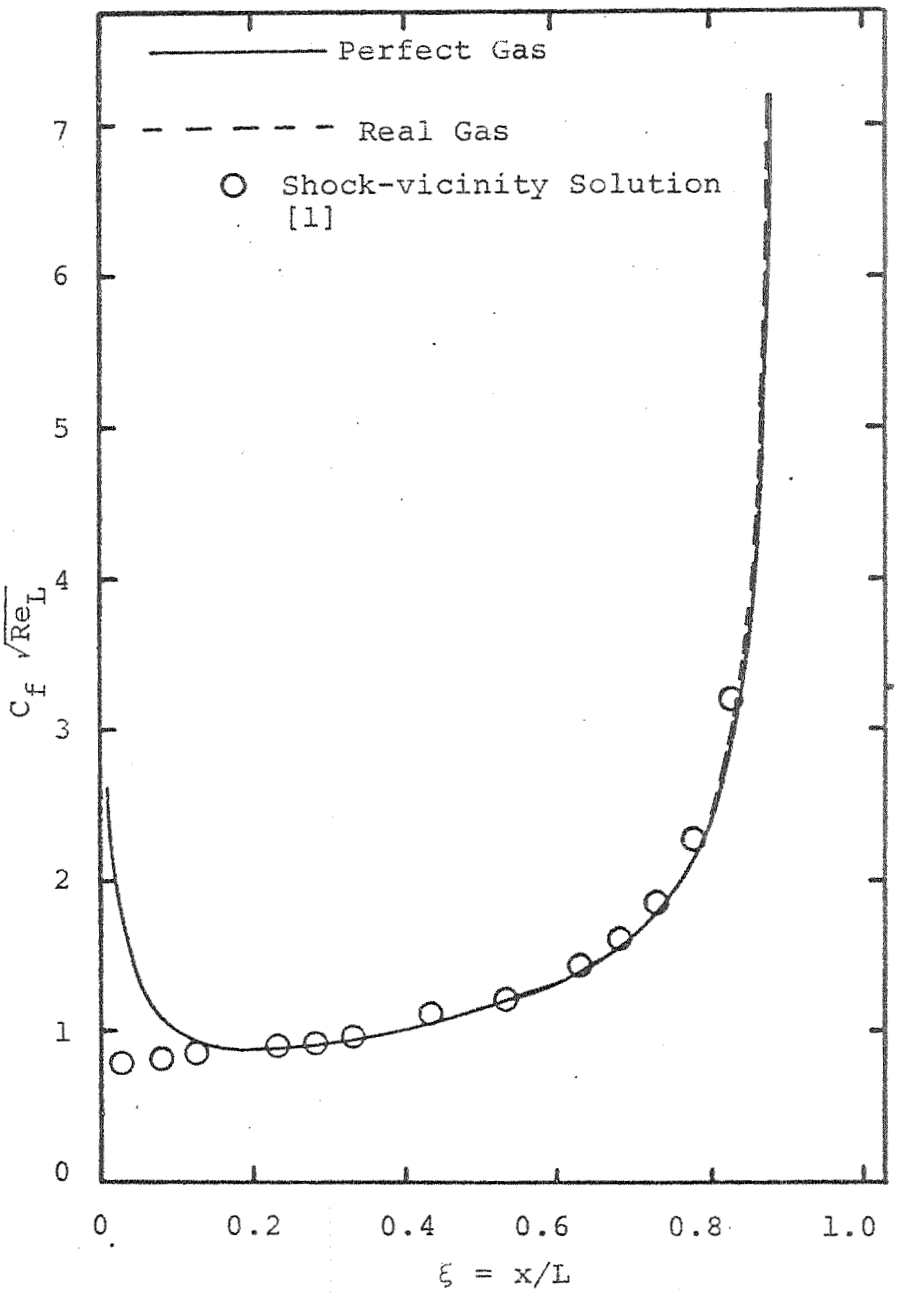

Figure 8. Comparison of Skin-Friction Coefficient with Shock-Vicinity Solution [1] for $M_s = 1.6$.

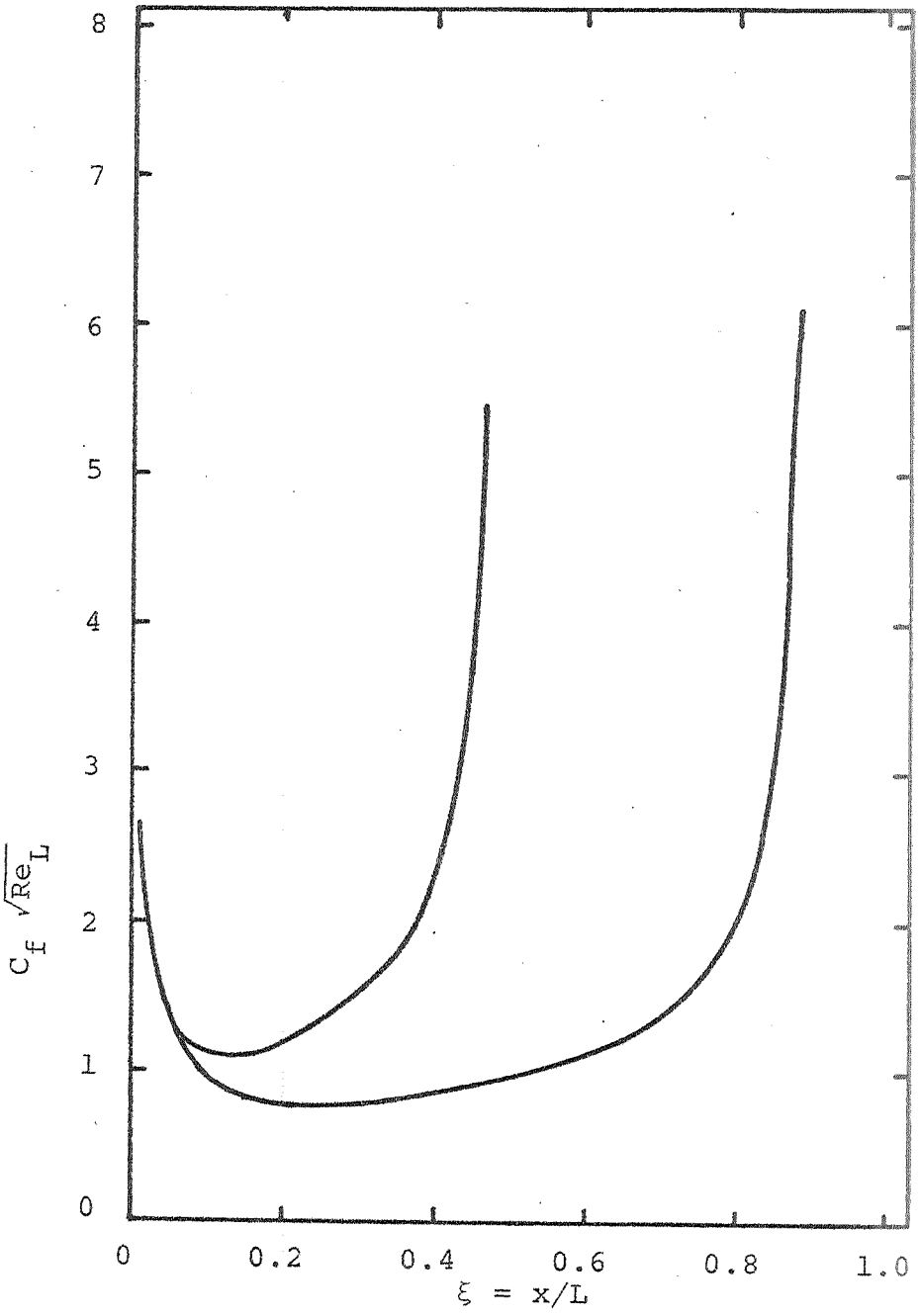

Figure 9. Skin-Friction Variation Along the Plate for Two Locations of the Shock; Perfect Gas, $M_s = 2.2$.

10 a comparison of the skin friction results for the complete and the shock-vicinity analyses is shown for a perfect gas with $M_s = 3.15$. Figure 11 shows the corresponding comparison assuming a real gas for both the complete and the shock-vicinity flows; it may be observed that the shock-vicinity results deviate slightly more than was noted in figure 10. The comparison shown in figure 12 is for the variation of skin friction for both a perfect and real gas with $M_s = 5$. The results show that the perfect gas model now yields a lower value of skin friction at all points on the plate.

The evaluation of the heat transfer at the wall is based upon the Nusselt number as given in equation (4.1g). Figure 13 shows the Nusselt number variation for both a perfect and real gas with $M_s = 1.6$ for the complete and the shock-vicinity solutions. It is seen that the shock-vicinity solution departs from the complete solution more than was observed previously in connection with skin friction variation. A comparison of the perfect and real gas solutions for shock wave Mach numbers of 2.2, 5, and 12 are shown in figures 14, 15, and 16, respectively. It is clear from these figures that the real gas departure from the perfect gas calculations becomes very large with increasing shock wave intensity. However, these figures also show that the present solution appears to be encountering numerical stability problems downstream of the shock wave location. Since the hump shown in these figures, which obviously increases with increasing values of M_s, was not encountered in the shock-vicinity calculations of reference [1] for the

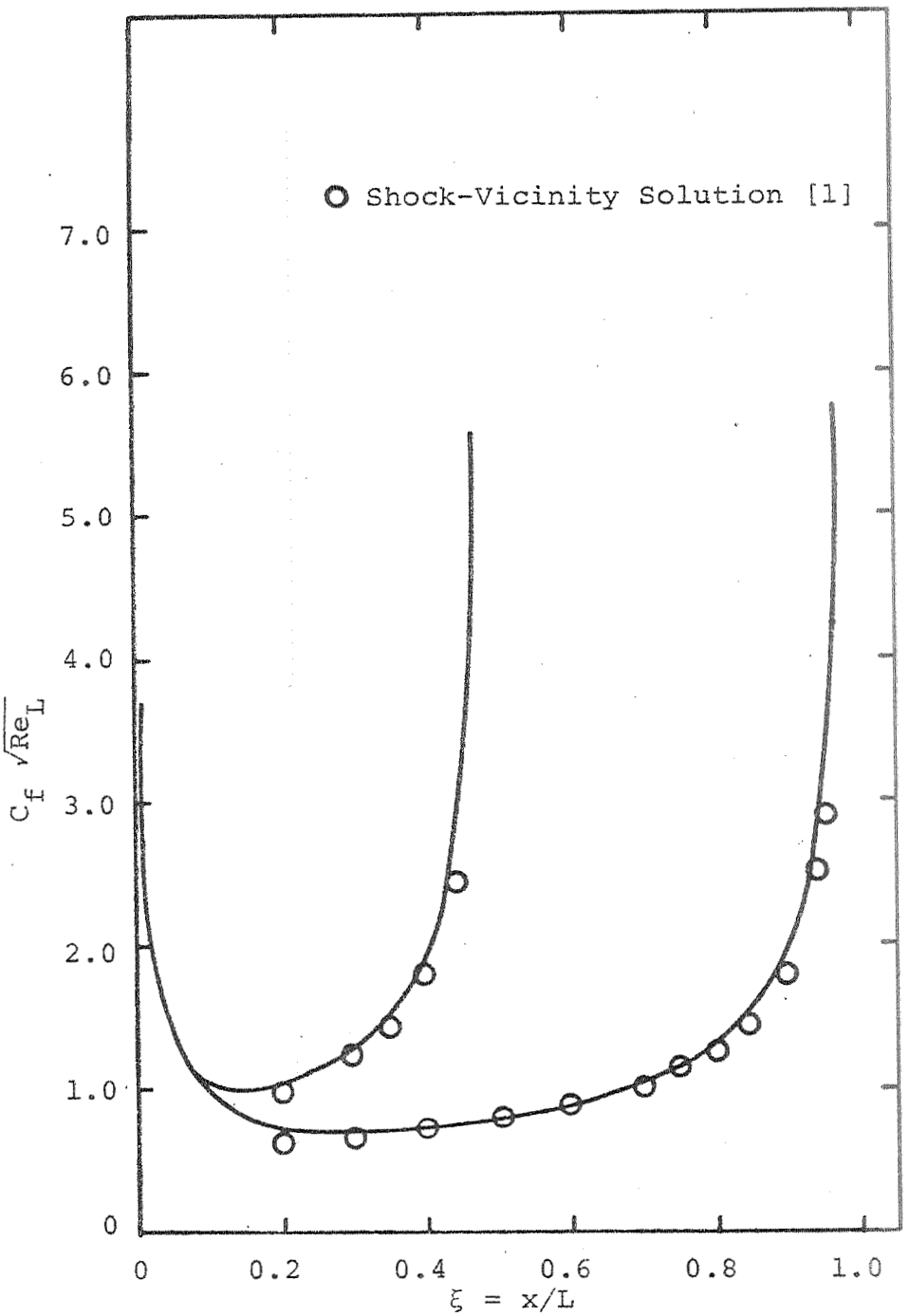

Figure 10. Comparison of Skin-Friction Coefficient with Shock-Vicinity Solution [1]: Perfect Gas, $M_s = 3.15$.

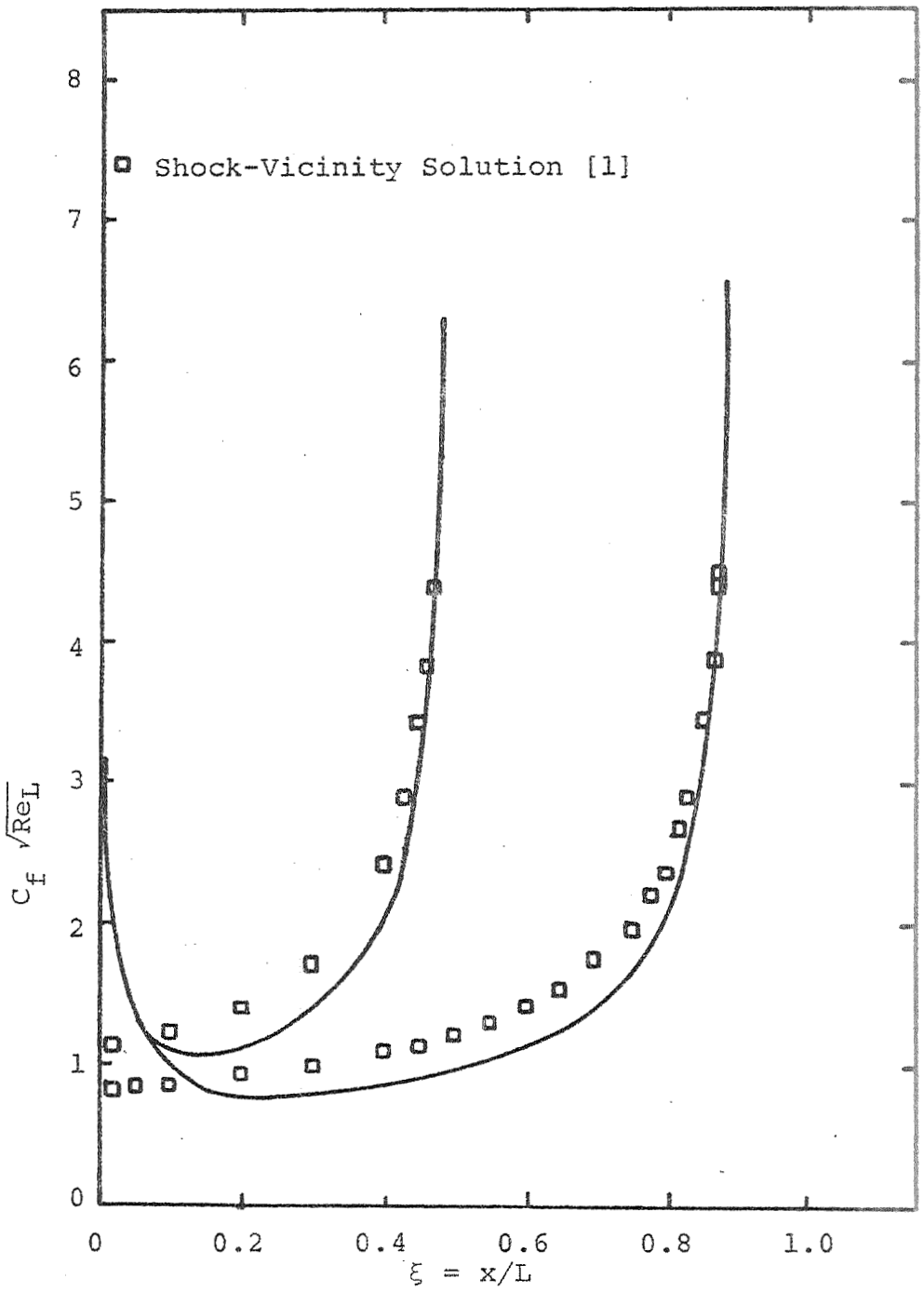

Figure 11. Comparison of Skin-Friction Coefficient with Shock-Vicinity Solution [1]: Real Gas, $M_s = 3.15$.

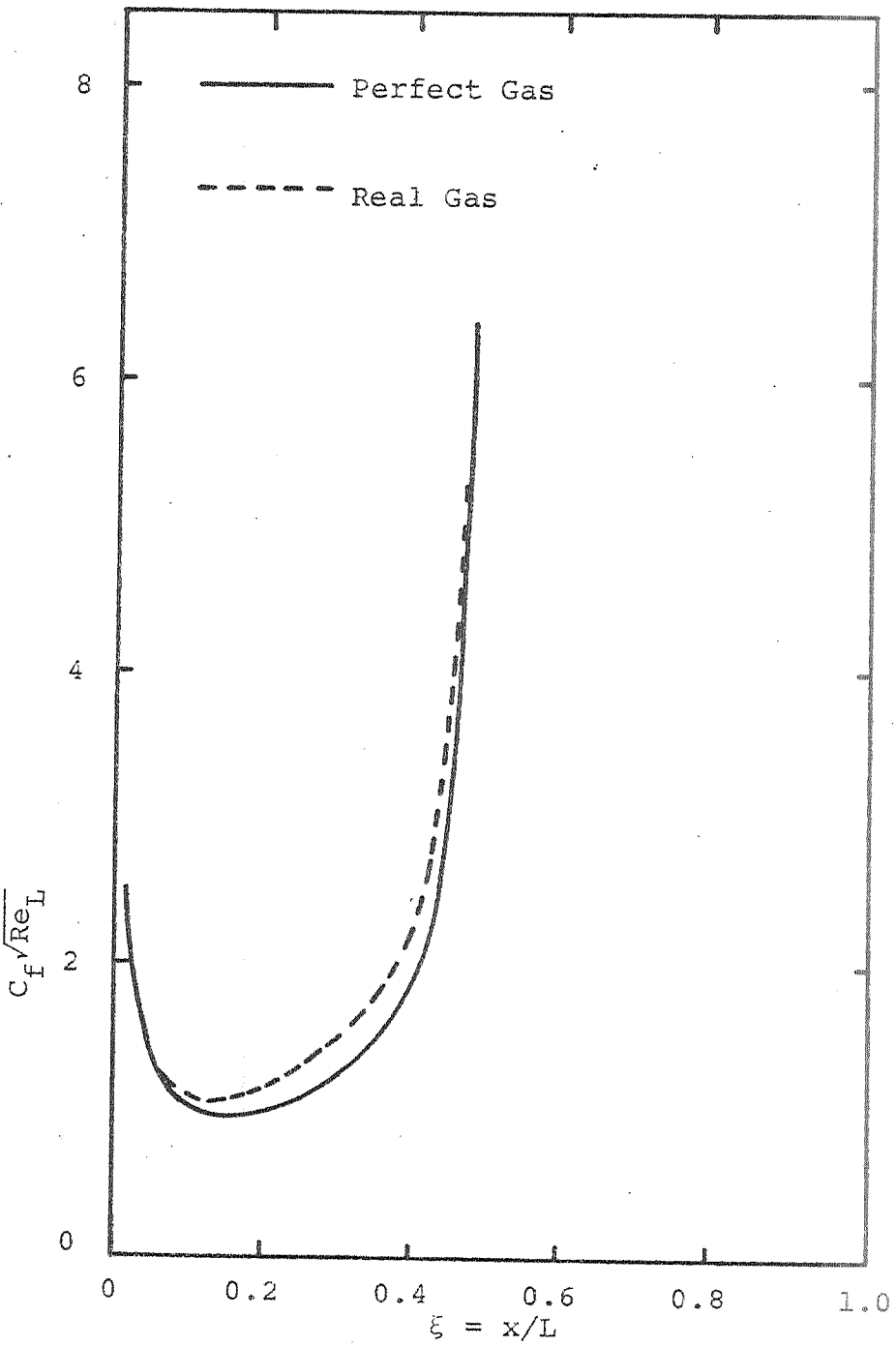

Figure 12. Comparison of Skin-Friction Coefficient for Perfect and Real Gas Solutions, $M_s = 5$.

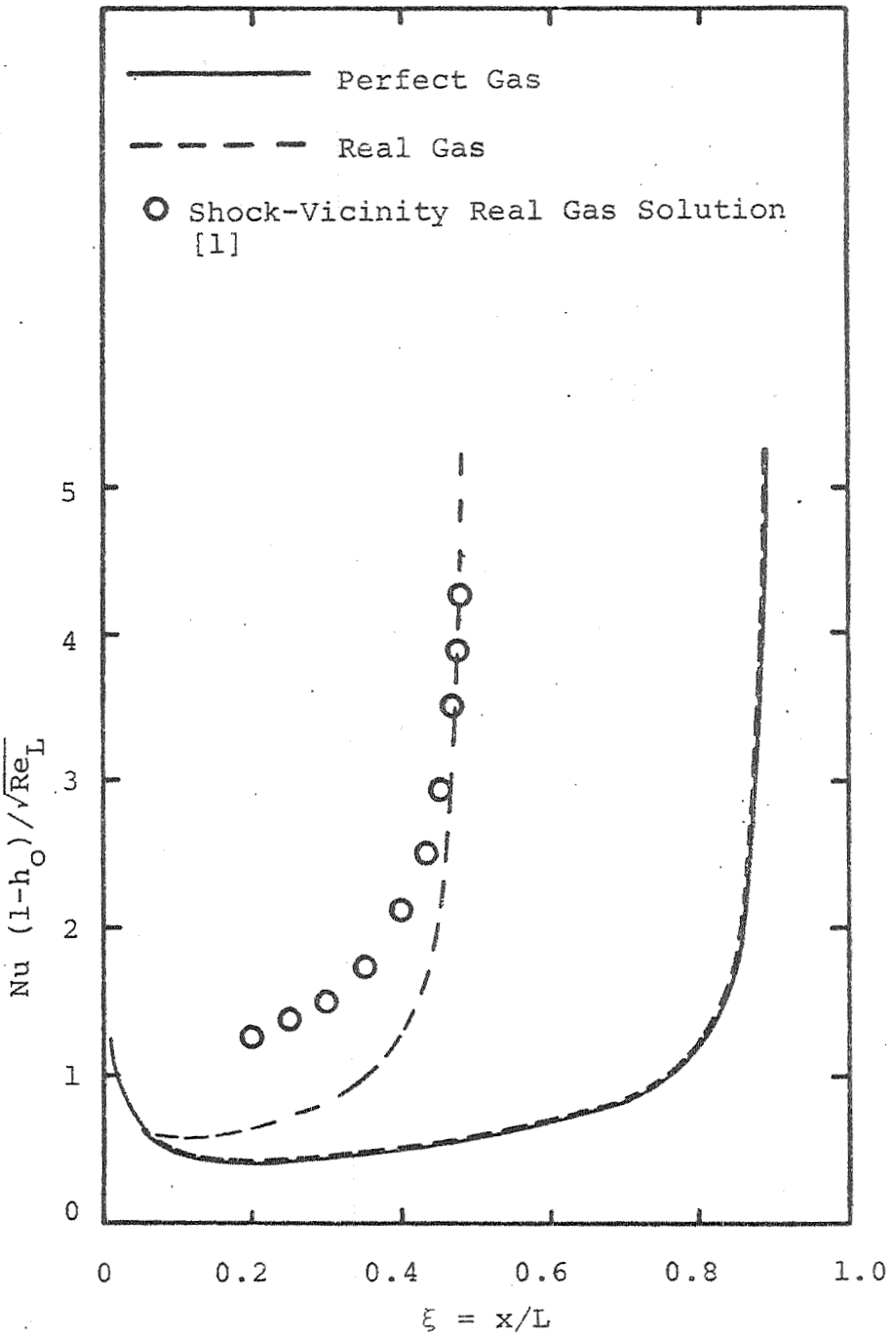

Figure 13. Comparison of Nusselt Number Distribution, $M_s = 1.6$.

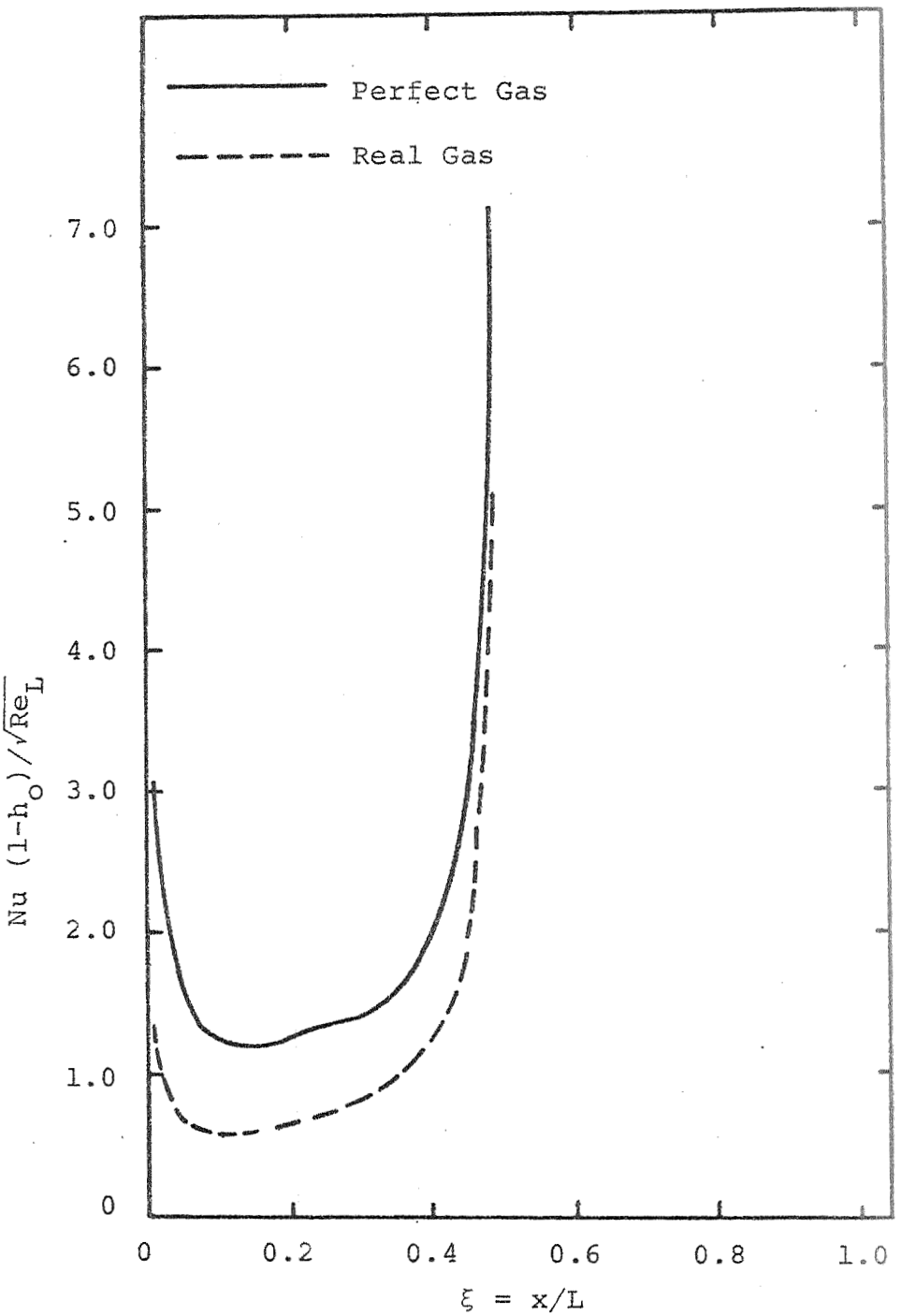

Figure 14. Comparison of Nusselt Number Distribution, $M_s = 2.2$.

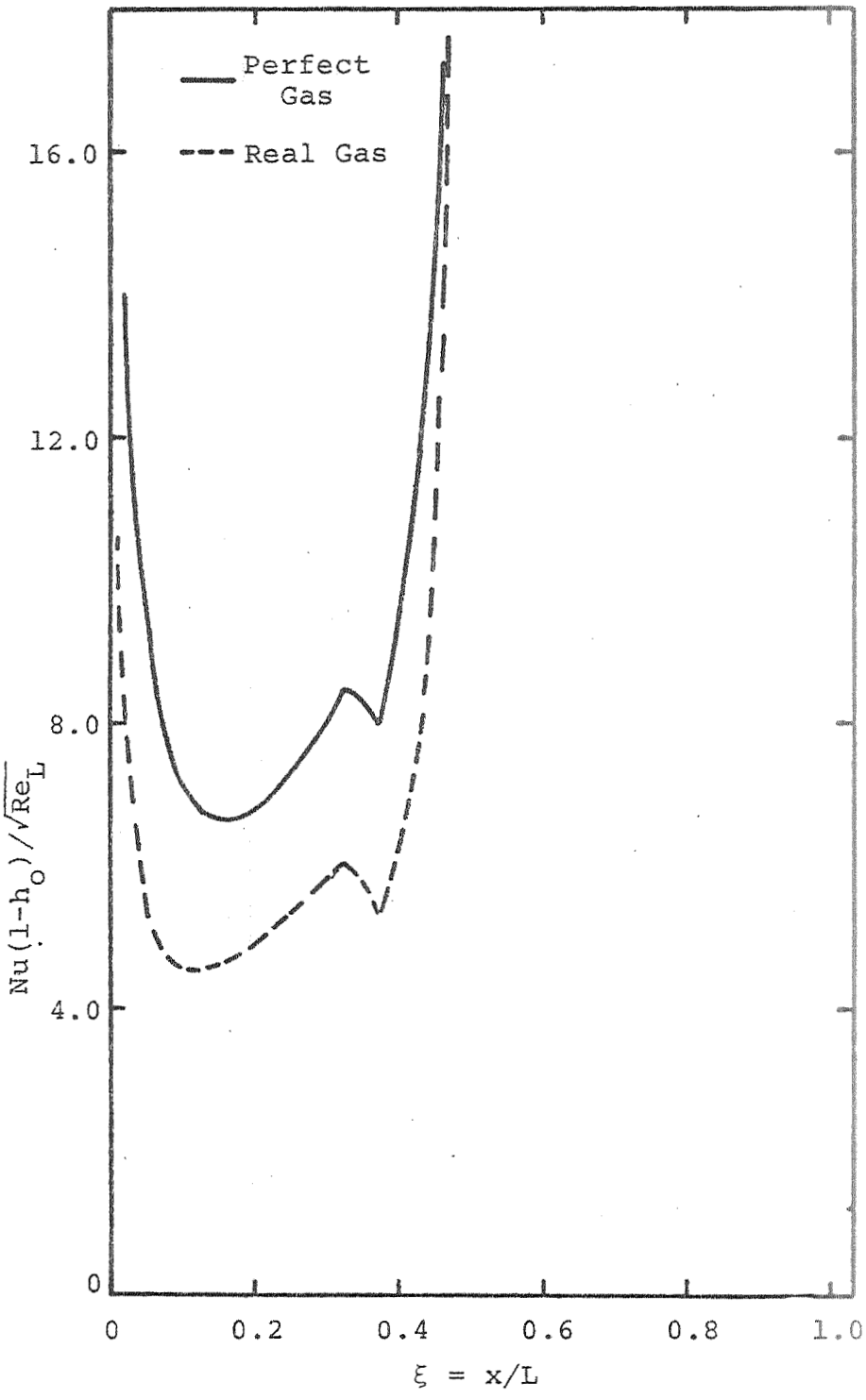

Figure 15. Comparison of Nusselt Number Distribution, $M_s = 5$.

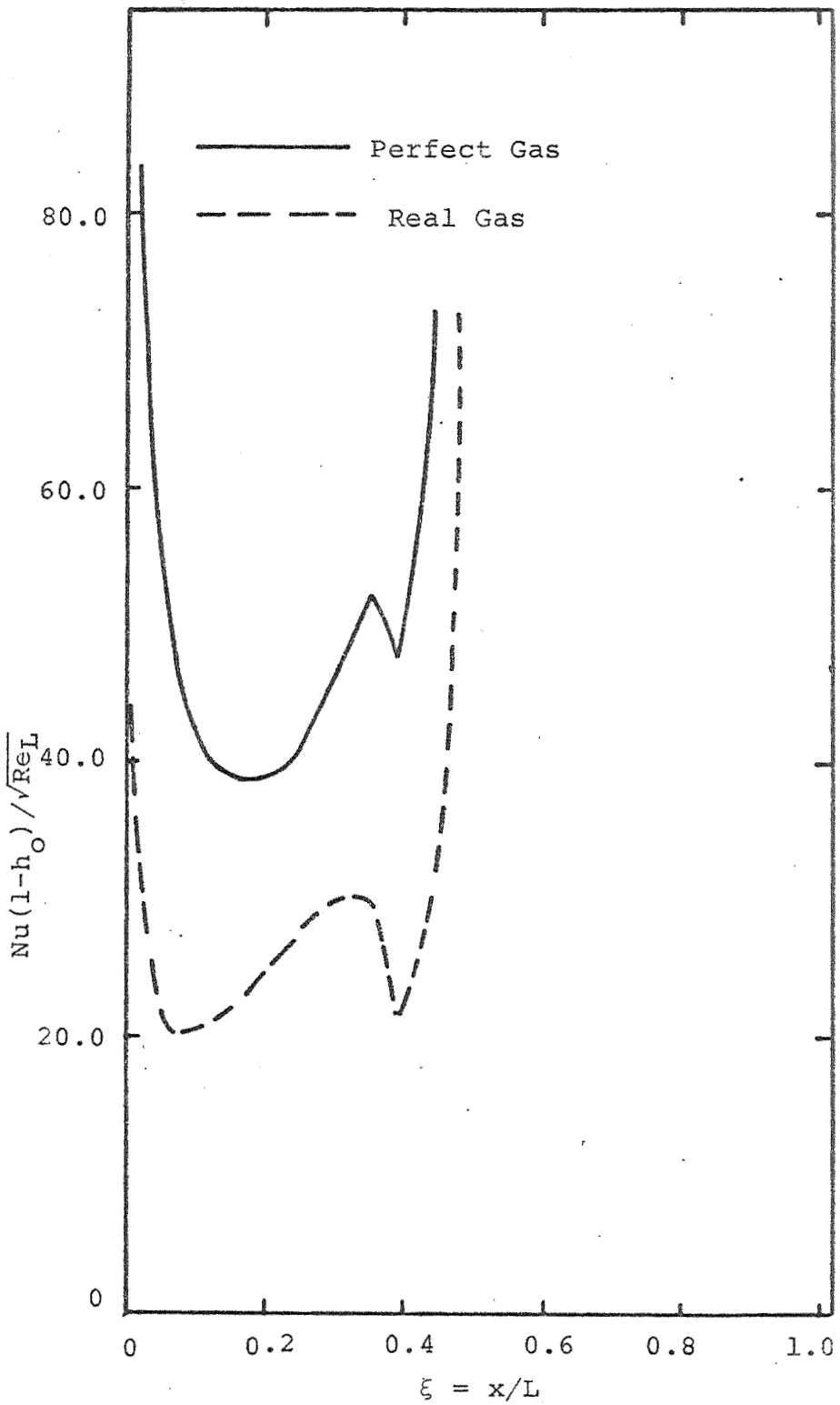

Figure 16. Comparison of Nusselt Number Distribution, $M_s = 12$.

corresponding shock intensities, the cause probably lies with the numerical smoothing procedure discussed earlier. Again, this point will have to be investigated in more detail in future work.

5. SUMMARY AND CONCLUSIONS

The complete problem of shock induced boundary-layer flow on a semi-infinite flat plate has been solved by a combined method of weighted residuals and finite difference technique. The present analysis was developed as a direct extension of the MWR second approximation given in reference [1] for the flow in the vicinity of the shock wave. By modifying the earlier work to account for the plate leading edge, and introducing a finite difference scheme to treat the resulting truly unsteady equations, solutions were obtained for typical boundary-layer parameters for both a perfect and real gas (nitrogen) for a range of shock wave Mach numbers from 1.6 to 12.

It was shown that the calculated boundary-layer thickness differs significantly from the shock-vicinity calculations of [1] except very close to the shock wave; of course, near the leading edge the shock-vicinity solution breaks down completely. It was also shown that the predicted asymptotic approach of the leading-edge flow to steady-state values (as the shock wave moves farther and farther along the plate) agrees very well with experimental results based on wall heat transfer measurements.

Results were also shown for the skin-friction coefficient and the Nusselt number for a variety of shock intensities and

shock wave locations for both a perfect and real gas calculations. As expected, it was shown that (i) the solutions agreed well with the shock-vicinity solutions near the shock wave, and (ii) the perfect and real gas solutions departed more and more from each other with increasing shock wave Mach numbers.

An unexpected anomology appeared in the calculations, to some extent for the boundary-layer thickness but very pronounced for the Nusselt number variation, as evidenced by a waviness or dipping of the predicted curves between the shock-wave location and the point where the respective curves showed a marked departure to their leading-edge value. This unusual behavior can probably be blamed on a numerical smoothing procedure that was incorporated into the analysis as a result of the parabolic nature of the original governing (boundary-layer) equations. The point needs further work and possibly could be resolved by considering a Navier-Stokes model for the flow, rather than the boundary-layer model presently employed.

6. REFERENCES

1. Abbott, D. E. and Ero, M. I. O.: Shock Induced Boundary Layer Over a Semi-Infinite Flat Plate. Part I: Flow in the Immediate Vicinity of the Shock Wave. Technical Report FMTR-70-1, School of Mechanical Engineering, Purdue University, January 1970.

2. Koob, S. J. and Abbott, D. E.: An Integral-Differential-Difference Method Analysis of Viscous Flow Over an Impulsively Accelerated Semi-Infinite Plate. Technical Report FMTR-68-2, School of Mechanical Engineering, Purdue University, December, 1968.

3. Lam, S. H., and Crocco, L.: "Shock Induced Unsteady Laminar Compressible Boundary Layer On a Semi-Infinite Flat Plate". Princeton University Report No. 428 AFOSR TN 58-581, AD 162-101, Sept., 1958.

4. Mirels, H.: Boundary Layer Behind Shock or Thin Expansion Wave Moving Into Stationary Fluid. NACA TN-3712. May, 1956.

5. Ahtye, W. F., and Peng, Tzy-Cheng: Approximations for Thermodynamic and Transport Properties of High Temperature Nitrogen with Shock-Tube Applications. NASA-TN D-1303, 1962.

6. Marvin, J. G., and Deiwert, G. S.: Convective Heat Transfer in Planetary Gases. NASA TR R-224. July, 1965.

7. Felderman, E. J.: Heat Transfer and Shear Stress in the Shock-Induced Unsteady Boundary Layer on a Flat Plate. AIAA Journal, Vol. 6, No. 3, March 1968, pp. 408-412.

8. Davies, W. R. and Bernstein, L.: Heat Transfer and Transition to Turbulence in the Shock-Induced Boundary Layer on a Semi-Infinite Flat Plate. J. Fluid Mechanics, Vol. 36, Part 1, 1969, pp. 87-112.